TARGET IDENTIFICATION USING ISAR IMAGING TECHNIQUES

A THESIS SUBMITTED TO
THE GRADUATE SCHOOL OF NATURAL AND APPLIED SCIENCES
OF
MIDDLE EAST TECHNICAL UNIVERSITY

BY

ERDİNÇ LEVENT ATILGAN

IN PARTIAL FULFILLMENT OF THE REQUIREMENTS
FOR
THE DEGREE OF MASTER OF SCIENCE
IN
ELECTRICAL AND ELECTRONICS ENGINEERING

DECEMBER 2005

Approval of the Graduate School of Natural and Applied Sciences

Prof. Dr. Canan ÖZGEN
Director

I certify that this thesis satisfies all the requirements as a thesis for the degree of Master of Science.

Prof. Dr. İsmet ERKMEN
Head of Department

This is to certify that we have read this thesis and that in our opinion it is fully adequate, in scope and quality, as a thesis for the degree of Master of Science.

Prof. Dr. Kemal LEBLEBİCİOĞLU
Co-Supervisor

Prof. Dr. Zafer ÜNVER
Supervisor

Examining Committee Members

Prof. Dr. Gülbin DURAL (METU,EE) _____

Prof. Dr. Zafer ÜNVER (METU,EE) _____

Prof. Dr. Kemal LEBLEBİCİOĞLU (METU,EE) _____

Assoc. Prof. Dr. Tolga ÇİLOĞLU (METU,EE) _____

Serkan SEVİM (M.Sc.) (ASELSAN) _____

I hereby declare that all information in this document has been obtained and presented in accordance with academic rules and ethical conduct. I also declare that, as required by these rules and conduct, I have fully cited and referenced all material and results that are not original to this work.

Name, Last name : Erdinç Levent, ATILGAN

Signature :

ABSTRACT

TARGET IDENTIFICATION USING ISAR IMAGING TECHNIQUES

Atılgan, Erdinç Levent
M.S., Department of Electrical and Electronics Engineering
Supervisor : Prof. Dr. Zafer Ünver
Co-Supervisor : Prof. Dr. Kemal Leblebicioğlu

August 2005, 93 pages

A proper time-frequency transform technique suppresses the blurring and smearing effect of the time-varying Doppler shift on the target image. The conventional target imaging method uses the Fourier transform for extracting the Doppler shift from the received radar pulse. Since the Doppler shift is time-varying for rotating targets, the constructed images will be degraded.

In this thesis, the Doppler shift information required for the Range-Doppler image of the target is extracted by using high resolution time-frequency transform techniques. The Wigner-Ville Distribution and the Adaptive Gabor Representation with the Coarse-to-Fine and the Matching Pursuit Search Algorithms are examined techniques for the target imaging system.

The modified Matching Pursuit Algorithm, the Matching Pursuit with Reduced Dictionary is proposed which decreases the signal processing time required by the Adaptive Gabor Representation. The Hybrid Matching Pursuit Search Algorithm is also introduced in this thesis work and the Coarse-to-Fine Algorithm and the Matching Pursuit Algorithm are combined for obtaining better representation quality of a signal in the time-frequency domain.

The stated techniques are applied on to the sample signals and compared with each other. The application of these techniques in the target imaging system is also performed for the simulated aircrafts.

Keywords : Inverse Synthetic Aperture Radar, Joint Time-Frequency Transform, Wigner-Ville Distribution, Matching Pursuit Algorithm, Adaptive Gabor Representation.

ÖZ

ISAR GÖRÜNTÜLEME TEKNİKLERİ İLE HEDEF BELİRLEME

Atılgan, Erdinç Levent
Yüksek Lisans, Elektrik Elektronik Mühendisliği Bölümü
Tez Yöneticisi : Prof. Dr. Zafer Ünver
Ortak Tez Yöneticisi : Prof. Dr. Kemal Leblebicioğlu

Ağustos 2005, 93 sayfa

Uygun bir zaman sıklık çevrim tekniği sayesinde, zamanda değişen Doppler değişiminin hedef görüntüsü üzerinde yarattığı bulanıklık ve lekeler azaltılabilir. Sıradan hedef görüntüleme sistemi Doppler değişim bilgisini alınan radar darbesinden Fourier çevrimi ile elde eder. Dönen hedefin Doppler değişimi zamanla değiştiği için oluşturulan görüntü bozuk olacaktır.

Bu tezde, hedefin Menzil-Doppler görüntüsü için gerekli olan Doppler değişim bilgisi, yüksek çözünürlüklü zaman sıklık çevrim teknikleri kullanılarak bulunmuştur. Wigner-Ville Dağılımı, Kabadan İnceye Algoritması ile Uyarlamalı Gabor Gösterimi, Uyum Kovalama Algoritması ile Uyarlamalı Gabor Gösterimi hedef görüntüleme sistemi için incelenen tekniklerdir.

Uyum Kovalama Algoritması önerilen "Kısıtlanmış Sözlük ile Uyum Kovalama Algoritması" ile geliştirilmeye çalışılmıştır. Böylece Uyarlamalı Gabor gösteriminin işaret işleme süresi kısaltılmıştır. Bu tez çalışmasında ayrıca Bileşik Uyum Kovalama Algoritması tanıtılmış ve işaretin zaman-sıklık bölgesindeki gösterimini daha iyi hale getirmek için Kabadan İnceye Algoritması ile Kısıtlanmış Sözlük ile Uyum Kovalama Algoritması birleştirilmiştir.

Sözü geçen teknikler örnek işaretler üzerinde uygulanmış ve birbirleri ile karşılaştırılmıştır. Tekniklerin hedef görüntüleme sistemindeki uygulamaları taklit hedef kullanılarak gerçekleştirilmiştir.

Anahtar Kelimeler : Ters Yapay Ağız Aralıklı Radar, Tümleşik Zaman-Sıklık Çevrimi, Wigner-Ville Dağılımı, Uyum Kovalama Algoritması, Uyarlamalı Gabor Gösterimi.

To Yasemin

ACKNOWLEDGMENTS

I wish to express my sincere gratitude and appreciation to Professor Zafer Ünver, for his keen interest, guidance, endless patience, and support during this work. I would like to thank Professor Kemal Leblebicioğlu for his valuable comments and criticisms and also I would like to thank Assoc. Professor Gülbin Dural, Assoc. Professor Tolga Çiloğlu for serving on my committee.

I thank Serkan Sevim and Oral Dinçer for their guidance and valuable supports.

I am grateful to Yasemin Kayhan and her family for their constant support, encouragement, and above all, for instilling me the love of learning.

I thank my parents for their support and words of encouragement, who were very patient and helped me at every point of my M.Sc. study.

TABLE OF CONTENTS

LIST OF FIGURES

FIGURES

CHAPTER 1

INTRODUCTION

1.1 Basics of Target Imaging

Radar has been used for target detection. Besides this, by using the scaling in amplitude and shift in phase of the scattered radar waveform from the target, imaging the moving targets becomes possible [1][2]. The aim of the imaging radar is to generate an image of the scene illuminated within the radar antenna beam width.

The quality of the image highly depends on the range and cross-range resolution of the radar [1]. The range resolution is the minimum distance which can be resolved by the radar between two adjacent point scatterers along the radar line-of-sight (LOS). Two adjacent point scatterers can be differentiated from each other if the reflected radar pulses from each can be received as two different pulses. Therefore, the radar range resolution is inversely proportional with the radar pulse width and directly proportional with the bandwidth of the radar pulse [5].

The cross-range resolution is the minimum distance which can be resolved by the radar between two point scatterers on the plane to which the radar LOS is normal. The cross-range resolution is related with the radar antenna beam width. Thinner the antenna beam width, better the cross-range resolution. Figure 1.1 shows the relation of antenna beam width and cross-range resolution. Since the beam width

of the antenna is inversely proportional with the length of the antenna aperture size, using the real array radar for target imaging is not feasible. To achieve high cross-range resolution without using a large physical antenna aperture, synthetic array radar processing is widely used [5][6].

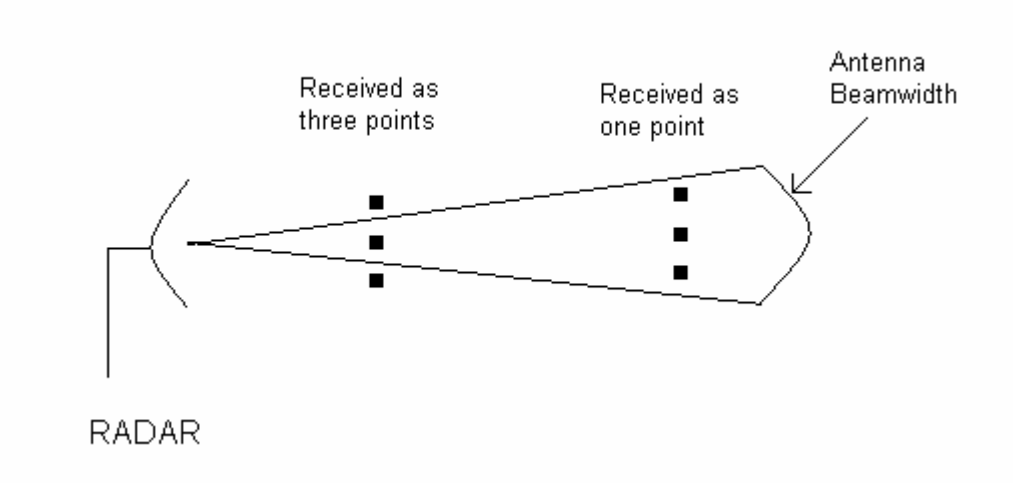

Figure 1.1: Antenna beam width and cross-range resolution.

A closely related concept to synthetic aperture radar (SAR) is inverse synthetic aperture radar (ISAR). Basic difference between SAR and ISAR is the usage of the radar. In SAR applications, the imaging radar is on a moving platform and the target is stationary. In ISAR applications, the target to be imaged moves and the radar is stationary. Therefore, SAR is used for generating images of terrain while ISAR is used for imaging aircrafts or ships.

ISAR utilizes the Doppler information to acquire cross-range resolution [8][12]. By using the Doppler spectra of the received radar pulse scattered from the target, Doppler frequency shifts of adjacent point scatterers can be differentiated. Therefore, the distribution of the scatterers on the target can be mapped on to

plane, called the imaging plane, whose grids are determined by the range and cross-range resolution of the radar [5].

1.2 Target Imaging Methods

The conventional method for obtaining Doppler spectra of the received pulse is to use the Fourier transform, assuming the Doppler frequency shifts during imaging time are constant [1]. It is also assumed that the point scatterers on the target which will be imaged do not drift out from their resolution cells on the imaging plane [6][8][13]. (See Figure 1.2.)

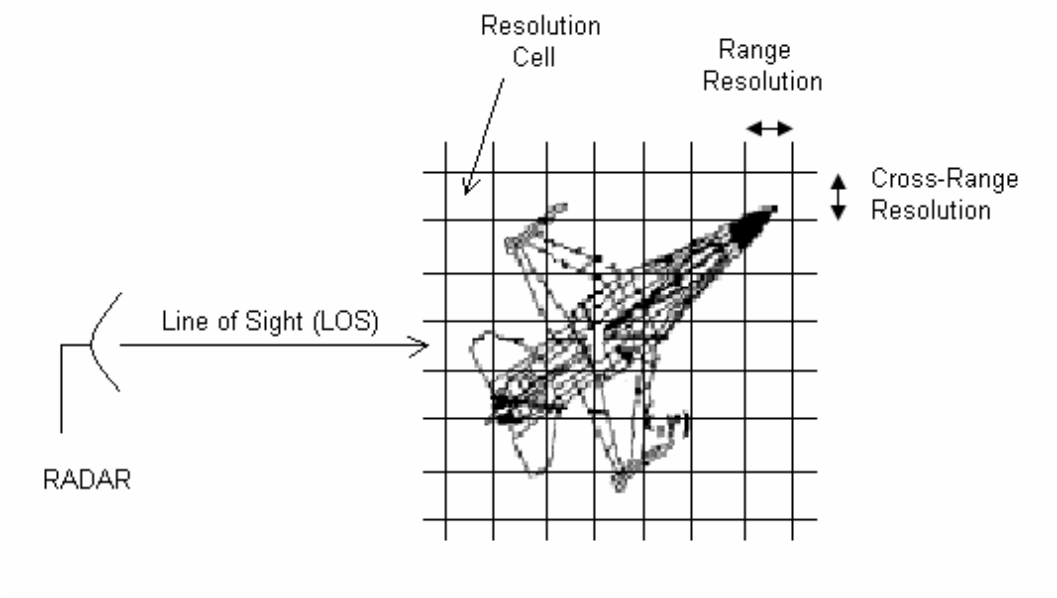

Figure 1.2: Resolution cell on target imaging plane.

If the Doppler frequency shifts are time-varying or the scatterers drift out from their resolution cells, the Doppler spectrum obtained by the Fourier transform will be smeared and the obtained target image will be blurred [14][20].

To obtain a clear image, the scatterers that drift out from their resolution cells should be pulled back into their grids. This process, called the range tracking, still not enough for target imaging. If the Doppler frequency shifts of scatterers are time-varying, then the Doppler tracking process should also be applied for phase compensation.

If the target exhibits a smooth motion, the range tracking (the standard motion compensation) may be enough for obtaining a clear image. However, when the target exhibits a complex motion, like rotation or maneuvering, the standard motion compensation will not be enough [15]. In this case, more complicated motion compensation procedures are required.

The restrictions on target imaging can be lifted by using a time-frequency transform instead of the Fourier transform [8]. By replacing the Fourier transform with a high-resolution time-frequency transform, the time varying Doppler frequency shifts will not disturb the image much, and there will be no need for complicated motion compensation procedures.

The time-frequency transform is an efficient way to resolve the image blurring problem caused by the time-varying Doppler shifts, and any time-frequency transform can be a candidate. However, to improve the image quality, the selected time-frequency transform should have high resolution in both time and frequency domain. In addition, the selected time-frequency transform should reflect the instantaneous frequency content of the analyzed signal accurately.

The Wigner-Ville Distribution (WVD) is a good candidate for target imaging [16]. However, the main drawback of the WVD is cross-term interference. When the signal contains more than one frequency component, the WVD will generate cross-term that occurs in the middle of every two frequency components of the signal on the time-frequency plane [7][9]. Although the cross-term has limited energy as compared to the main frequency components of the signal, the effect of it on quality of image may obscure the beneficial details of the image. Due to high resolution property, the WVD can not be discarded for target imaging, and by using proper signal decomposition methods, the advantages of WVD can be used for target imaging.

The Adaptive Gabor Representation (AGR) is one of the high resolution Joint Time-Frequency Transform (JTFT) techniques which utilizes the WVD without suffering from the cross-term interference [10][11]. The AGR decomposes the signal into a family of Gaussian modulated exponential elementary functions called the Gabor elementary functions. The elementary functions are very well localized in both time and frequency domains and their bandwidths are adaptable to match the local behavior of the signal. The main drawback of the method is the signal processing time. Since the method depends on adaptive decomposition of the signal, finding the accurate bandwidth for elementary functions which best matches with the signal may take time, and hence the processing time will be dependent on the signal to be analyzed.

In order to use the AGR in target imaging, the fast searching techniques are used for finding the best elementary Gabor functions. One of the applied search methods is the Coarse-to-Fine Search Algorithm (MP-CFS) [11]. The method starts to search with a wide Gabor function in the time domain and decreases the width of the elementary function step by step. The Coarse-to-Fine search technique spends much of the processing time for finding the best time

localization of the elementary function. After the time center of the elementary function is found, its frequency center is determined by using the Fourier transform.

As an alternative and better technique, the Matching Pursuit (MP) Algorithm can be considered for searching Gabor elementary functions [17]. The MP Algorithm uses a predefined elementary function dictionary for decomposing the given signal. Therefore, the method does not spend much processing time for finding the time center of the elementary function. The method just tries to select the best Gabor function from the dictionary by using an inner product operation.

Although the MP Algorithm is a fast searching technique, the dimension of the dictionary grows rapidly with the number of points taken from the signal to be decomposed. The constructed dictionary will be redundant in many cases, so using the MP Algorithm with a huge dictionary will not be feasible. Therefore, the Matching Pursuit with reduced dictionary (MP-RD) searching technique is proposed in this study for using the advantages of the MP Algorithm. The dictionary of the MP Algorithm is tried to be constructed by using almost independent elementary functions, thereby reducing the dimension of the dictionary to a proper level.

The MP-RD Algorithm makes the MP Algorithm feasible for running on a computer, but the details of the time-frequency representation of the signal is sacrificed. Since the details on the obtained target image can be important for the identification, another new approach is also studied. The MP-CFS shows good performance for the details of the signal on the time-frequency plane and the MP-RD gives the desired reduction on signal processing time. Hence the Hybrid-MP Algorithm is constructed by combining the two searching algorithms. In the Hybrid-MP, the MP-RD Algorithm tries to decompose the signal obtained by

running the CFS Algorithm up to a predefined iteration limit. Therefore, while the processing time is decreased, the quality of the obtained images is improved.

1.3 Outline

Chapter 2 explains the resolution terms for radar and the basic processes for obtaining the ISAR image of the target by using the Fourier transform. In Chapter 3, the usage of the time-frequency transform for the target imaging is introduced and some properties of the Wigner-Ville Distribution are explained. Chapter 4 introduces the adaptive signal decomposition technique, the Adaptive Gabor Representation. The searching techniques for the Adaptive Gabor Representation, the Coarse-to-Fine Search Algorithm and the Matching Pursuit Search Algorithm, are explained and two more algorithms, the Matching Pursuit with Reduced Dictionary and the Hybrid Matching Pursuit algorithms, are also introduced in Chapter 4. The performances of the proposed search algorithms are tested by using some example signals in Chapter 5. Chapter 5 also includes the application of these techniques for the target imaging system. Finally, Chapter 6 gives the conclusion for the study.

CHAPTER 2

CONVENTIONAL TARGET IMAGING METHOD

2.1 Introduction

In this chapter, radar range and cross-range resolution terms are briefly explained. Also Range-Doppler imaging by using 2-D Fourier transform is investigated, and the relation between the image quality and the radar resolutions is established. The usage of stepped frequency radar on target imaging is shown by using some examples.

2.2 Radar Range Resolution

The range resolution of radar can be defined in terms of its ability to resolve point targets that are separated along the range direction from the radar. For finding the range resolution expression of the radar, assume that the radar transmits a constant frequency and constant amplitude pulse, $s_T(t)$, to two different point scatterers located along the radar line-of-sight (LOS). The pulse shape of the radar can be written as follows,

$$s_T(t) = \sin(2\pi f_c t) w(t - \frac{T}{2}) \tag{2.1}$$

where f_c is the radar center frequency in Hertz and $w(t)$ is the window function given as,

$$w(t) = \begin{cases} 1 & for \quad -\frac{T}{2} \le t \le \frac{T}{2} \\ 0 & for \quad elsewhere \end{cases} \tag{2.2}$$

To realize that there are two different point scatterers along the radar LOS, the reflected pulses from the scatterers should be differentiated from each other as shown in Figure 2.1 Therefore, the minimum time shift amount between the two reflected pulses should be at least the duration of the sent pulse, T .

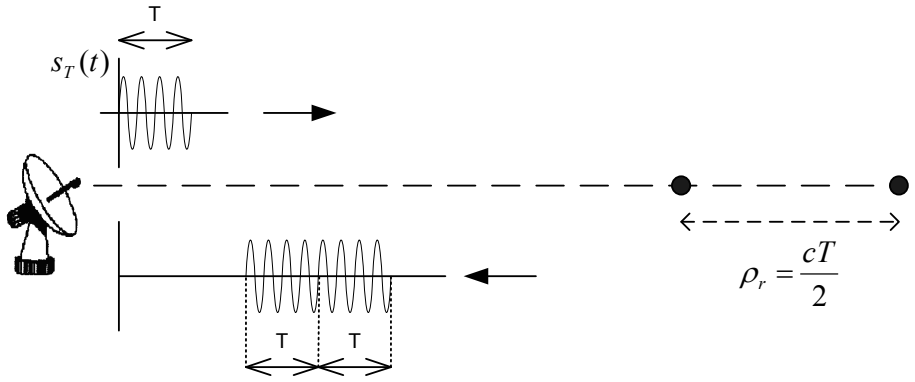

Figure 2.1: Sent and received radar pulses.

Hence the minimum distance between the point scatterers that can be differentiated by the radar can be expressed as follows [5],

$$\rho_r = \frac{cT}{2} \tag{2.3}$$

where c is the propagation speed of the radar pulse.

Since there is a strict relation between the duration and the bandwidth of the pulse, the range resolution expression can be rewritten by using the bandwidth of the sent pulse. The bandwidth of the transmitted pulse, which is also called the radar bandwidth, can be found by observing the Fourier transform of the transmitted pulse, $S_T(f)$, as shown in Figure 2.2.

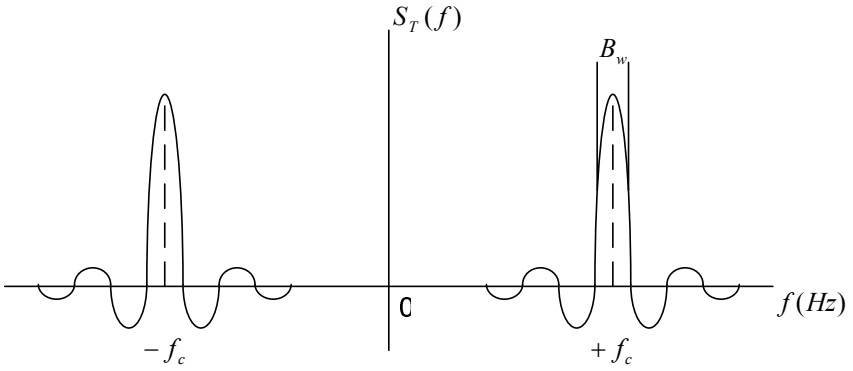

Figure 2.2: Fourier transform of $s_T(t)$.

Since $S_T(f)$ is frequency shifted version of the Fourier transform of window function, the radar bandwidth is nothing but the bandwidth of the window function of the transmitted pulse. The Fourier transform of the window function is given as,

$$W(f) = T\frac{\sin(\pi fT)}{\pi fT} \tag{2.4}$$

The bandwidth of the window function, B_w, can be taken as the first zero-crossing point of $W(f)$ shown in Figure 2.3,

$$B_w = \frac{1}{T} \tag{2.5}$$

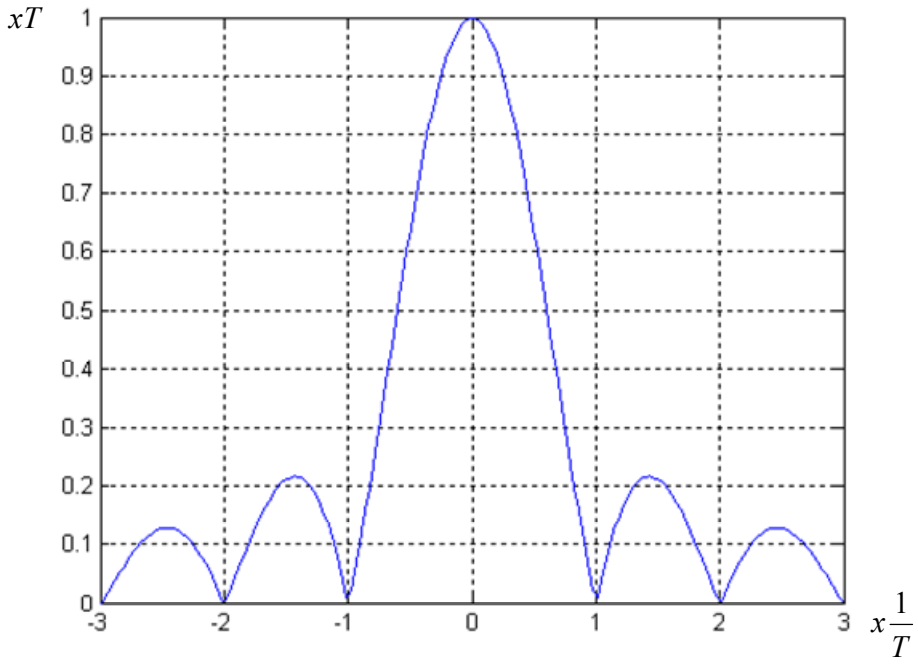

Figure 2.3: The magnitude of $W(f)$.

Therefore, the range resolution given by (2.3) can be rewritten by using (2.5) [5],

$$\rho_r = \frac{c}{2B_w} \tag{2.6}$$

2.3 Radar Doppler Resolution

The radial velocity of a point scatterer causes the frequency change in received pulse which is called the Doppler shift. Radar Doppler resolution refers to ability of the radar to resolve the Doppler shifts produced by two point scatterers moving at different radial velocities.

Assume that the radar transmits a pulse, $s_T(t)$,

$$s_T(t) = \exp(j2\pi f_c t) \tag{2.7}$$

The transmitted pulse will be reflected from a point scatterer which is moving along the radar LOS with constant velocity, v_R, as shown in Figure 2.4.

The received pulse, $s_R(t)$, will be time-shifted version of the transmitted pulse and the amount of time-shift will depend on the range, $r(t)$, between the radar and the point scatterer,

$$s_R(t) = \exp\left(j2\pi f_c (t - \frac{2r(t)}{c}) \right) = \exp(j\phi(t)) \tag{2.8}$$

The frequency of the received pulse, f_R, can be found by taking the derivative of the phase function with respect to time [3][8],

$$f_R = \frac{1}{2\pi}\frac{\partial\phi(t)}{\partial t} = f_c - \frac{2f_c}{c}\frac{\partial r(t)}{\partial t} = f_c - \frac{2f_c v_R}{c}$$

Therefore, the Doppler shift, f_D, produced by a single point scatterer with constant radial velocity v_R is expressed as,

$$f_D = \frac{2 f_c v_R}{c} = \frac{2 v_R}{\lambda} \tag{2.9}$$

where λ is the wavelength; and since v_R is much smaller than c, f_c is much larger than f_D.

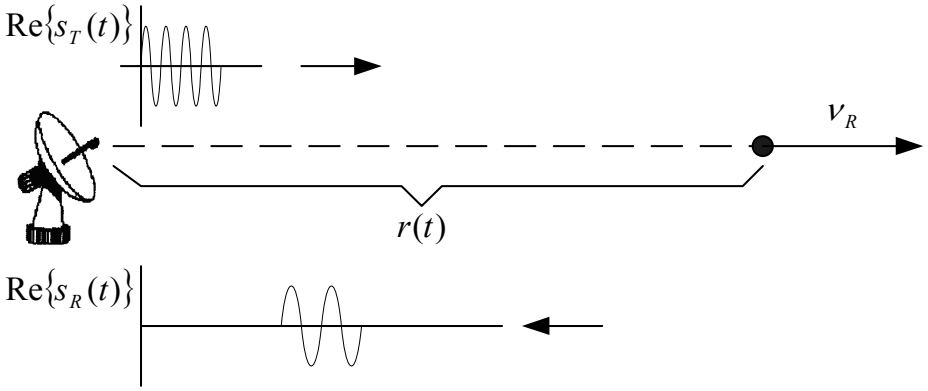

Figure 2.4: Moving point scatterer and received pulse.

The radar Doppler resolution depends on the observation time of the target. The observation time can be defined as the total duration of the transmitted pulse or pulse train to the target. For explaining the relation between observation time and Doppler resolution, assume that the radar transmits a pulse train which is composed of N pulses to two different point scatterers moving with different radial velocities, v_{R_1} and v_{R_2}. The duration of N pulses are taken as T_N as shown in Figure 2.5.

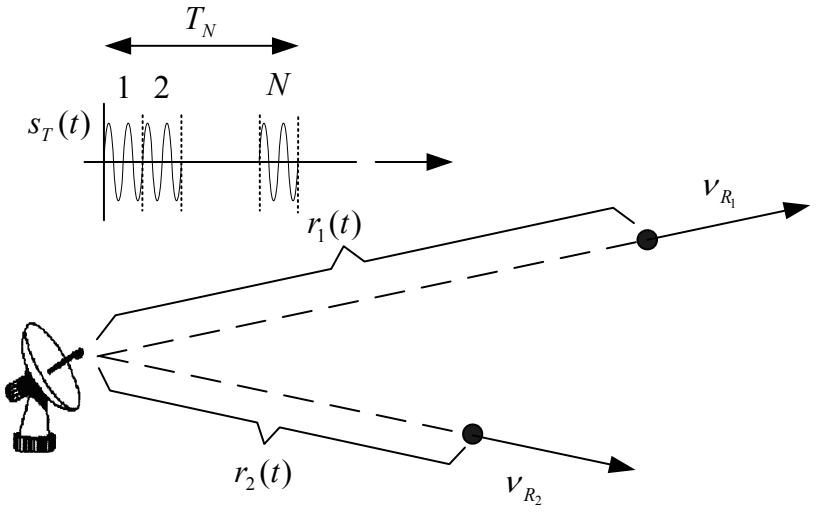

Figure 2.5: Two point scatterers with different radial velocities.

Since the radial velocities of point scatterers are different, their corresponding Doppler shift amounts, f_{D_1} and f_{D_2}, will also be different and the received signal will be sum of two different frequency signals, $s_{R_1}(t)$ and $s_{R_2}(t)$. (See Figure 2.6.)

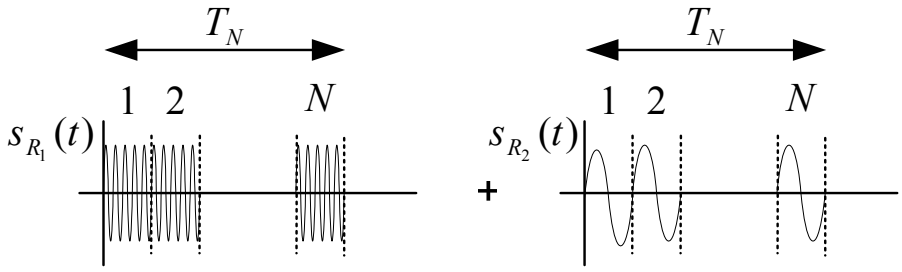

Figure 2.6: Components of received signal.

To identify the two peaks in the Fourier transform of the received signal, the minimum difference between the Doppler shifts of the components of the received signal should be $1/T_N$, which is reciprocal of the observation time, as shown in Figure 2.7.

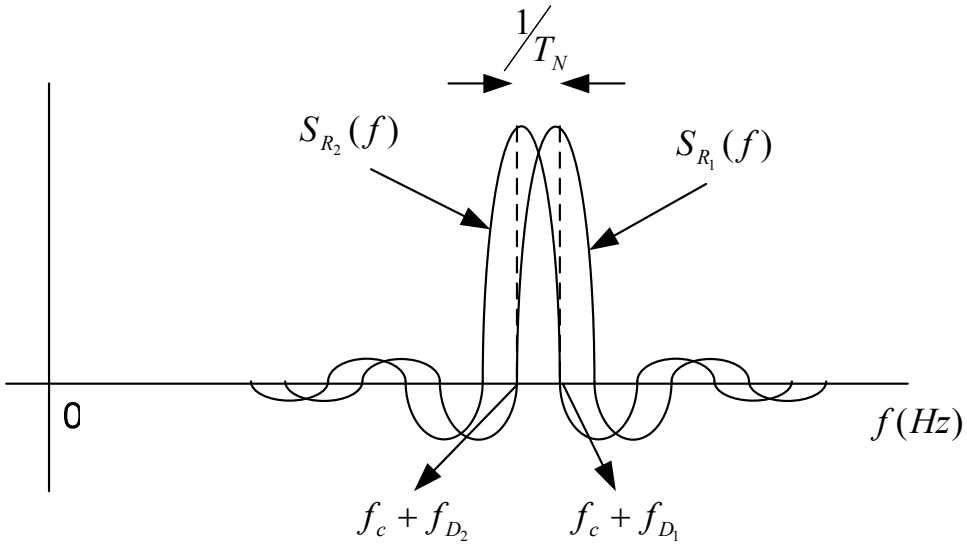

Figure 2.7: Fourier transforms of components of received signal.

Hence the radar Doppler resolution, Δf_D, can be written as [1],

$$\Delta f_D = \frac{1}{T_N} \tag{2.10}$$

2.4 The Range-Doppler Imaging

The target to be imaged can be modeled as a combination of point scatterers; the radar imaging is to determine the locations of the point scatterers on the target [3]. To try to find the coordinates of a point scatterer on the target, assume that the target, contained within the beam of the radar, is rotating about the point A at w radian per second and the radar is located at a distance r_a from the object. (See Figure 2.8.)

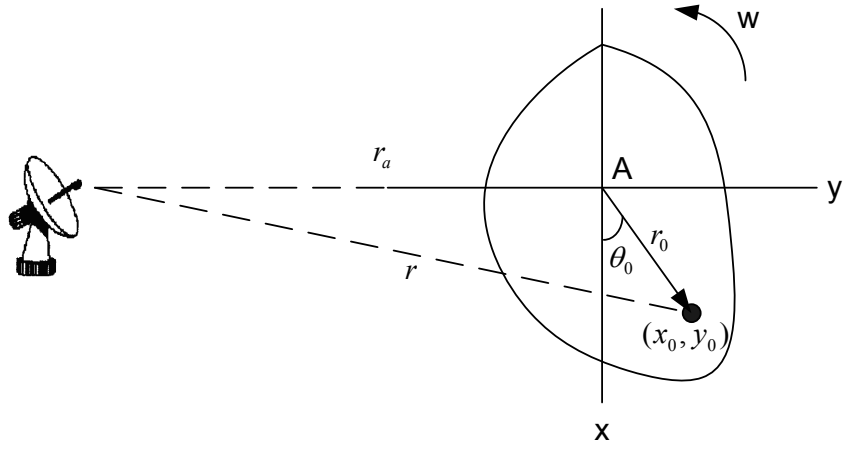

Figure 2.8: Point scatterer on rotating object.

The distance r of the point scatterer at location (x_0, y_0) to the radar can be written as,

$$r = \sqrt{(r_0^{\,2} + r_a^{\,2} + 2r_a r_0 \sin(\theta_0 + wt))} \tag{2.11}$$

where r_0 is the distance of point scatterer to the center of rotation, θ_0 is the initial angle of the point scatterer.

The distance from the radar to the center of rotation of the object, r_a, can be taken much larger than r_0. Therefore, (2.11) can be approximated as [1][3][8],

$$r \cong r_a + x_0 \sin(wt) + y_0 \cos(wt) \tag{2.12}$$

Since there is a relative motion between the radar and the target, there will be Doppler shift in the received signal. By using (2.9), the Doppler shift, f_D, of the returned signal is found as,

$$f_D = \frac{2v_R}{\lambda} = \frac{2}{\lambda}\frac{dr}{dt} = \frac{2x_0 w}{\lambda}\cos(wt) - \frac{2y_0 w}{\lambda}\sin(wt) \tag{2.13}$$

If the target observation time is taken short enough, the angle of rotation, (wt), of the target can be taken in the neighborhood of zero. Therefore, (2.12) and (2.13) can be approximated as [1][6][8],

$$r \cong r_a + y_0 \tag{2.14}$$

$$f_D \cong \frac{2x_0 w}{\lambda} \tag{2.15}$$

(2.14) and (2.15) show that the returned radar pulse can be processed for calculating the coordinates, (x_0, y_0), of the point scatterer of the target.

The resolution of the radar along y-axis and x-axis determines the resolution of the target image to be obtained. In other words, the range resolution of the radar gives the resolution of the image along y-axis, and the Doppler resolution of the radar gives the resolution of the image along x-axis, which is called the cross-range resolution. Since the range and the Doppler information are used for obtaining the target image, the process is called the Range-Doppler imaging [8][18].

If the measurable Doppler shift is Δf_D, then the obtainable cross-range resolution, ρ_c, of the image is related to Δf_D as,

$$\Delta f_D = \frac{2w\rho_c}{\lambda} \tag{2.16}$$

Since the Doppler resolution, Δf_D, is closely related with the target observation time, ΔT, (2.16) can be rewritten as,

$$\rho_c = \frac{\lambda}{2w\Delta T} = \frac{\lambda}{2\Delta\theta} \tag{2.17}$$

where $\Delta\theta$ is the angle through which the object rotates during the observation time.

Fine cross-range resolution implies a large $\Delta\theta$ and so long observation time; however (2.12) and (2.13) indicate that both the range and Doppler shift of a particular point scatterer can vary greatly over a long observation time. This means that during an observation time interval sufficiently long to give the desired cross-range resolution, point scatterers on the rotating object may move through several resolution cells. Therefore, the usual Range-Doppler imaging

implied by (2.14) and (2.15) will result in degraded image for the long observation time interval [6][8][13].

2.5 Target Imaging by Step Frequency Modulated Radar

There are several kinds of radar waveforms, which are proper for object imaging applications, like linear frequency modulated and chirp pulse waveforms. The used data set in imaging examples is taken from the stepped frequency modulated (SF) radar; therefore, the derivations for SF radar pulse can be helpful.

The SF radar pulse can be represented as [19],

$$s_T(t) = \cos\left[2\pi(f_0 + if_s)t\right]w(t) \tag{2.18}$$

where the index i is the frequency index, f_s is the step length of the frequency, f_0 is the carrier frequency of the pulse, $w(t)$ is the window function given in (2.2).

Figure 2.9 shows the process of target imaging by using the SF radar. The SF radar transmits a sequence of N bursts. Each burst consists of M pulses. The carrier frequency of each successive pulse in each burst is increased by a constant step frequency f_s.

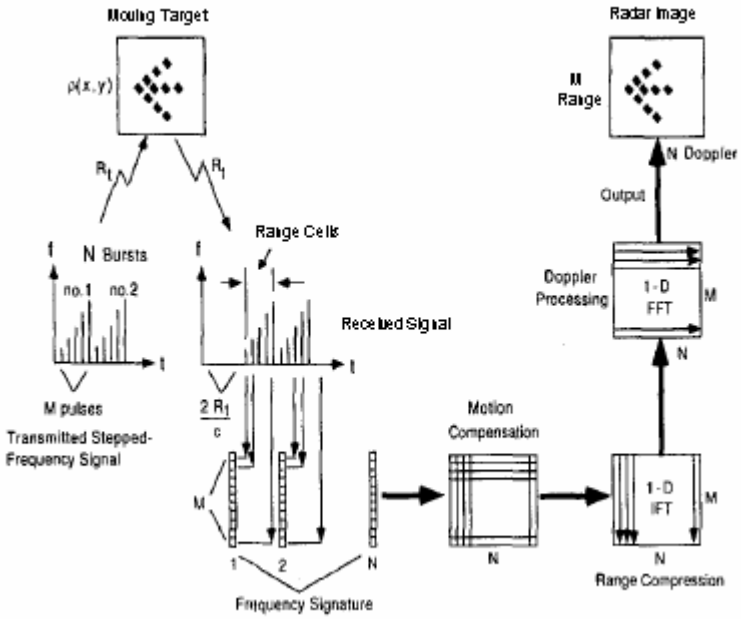

Figure 2.9: Stepped frequency radar imaging of moving target.

The radar bandwidth, M times the frequency step f_s, determines the radar range resolution, and total number of bursts N determines the cross-range or the Doppler resolution of the radar.

The derivation of the returned pulse from the overall target can be made simply by starting from a point scatterer on the target. Assume that the point scatterer at (x_0, y_0) coordinate modulate the amplitude of the sent radar pulse by the value proportional to the reflectivity function, $g(x, y)$, at (x_0, y_0).

The response of the differential area, $dxdy$, enclosing the point scatterer under consideration can be written as follows [19][12],

$$s_{R_0}(t) = Ag(x_0, y_0)\cos\left[2\pi(f_0 + if_s)(t - \frac{2r}{c})\right]w(t - \frac{2r}{c})dxdy \tag{2.19}$$

where A stands for the attenuation of the pulse, r is the distance from the radar to the point scatterer at (x_0, y_0).

Since the distance from the radar to the target is much larger than the target dimensions, the attenuation coefficient, A, is taken as constant.

By taking the integral of $s_{R_0}(t)$ over the area of the object, the returned pulse $s_R(t)$ can be found as [19],

$$s_R(t) = A\,\mathrm{Re}\left\{\int_{-\infty}^{+\infty}\int_{-\infty}^{+\infty} g(x,y)\exp\left\{j2\pi(f_0 + if_s)(t - \frac{2r}{c})\right\}dxdy\right\} \tag{2.20}$$

on the time interval

$$-\frac{T}{2} + \frac{2(r_a - L)}{c} < t < \frac{T}{2} + \frac{2(r_a + L)}{c} \tag{2.21}$$

where L denotes the radius of circular area in which the reflectivity function is non-zero. In other words, the circle with radius L encloses the total target area.

I-Q demodulation is applied at the receiver side to the received signal given by (2.20) to obtain a radar image [1][8][19]. (See Figure 2.10.)

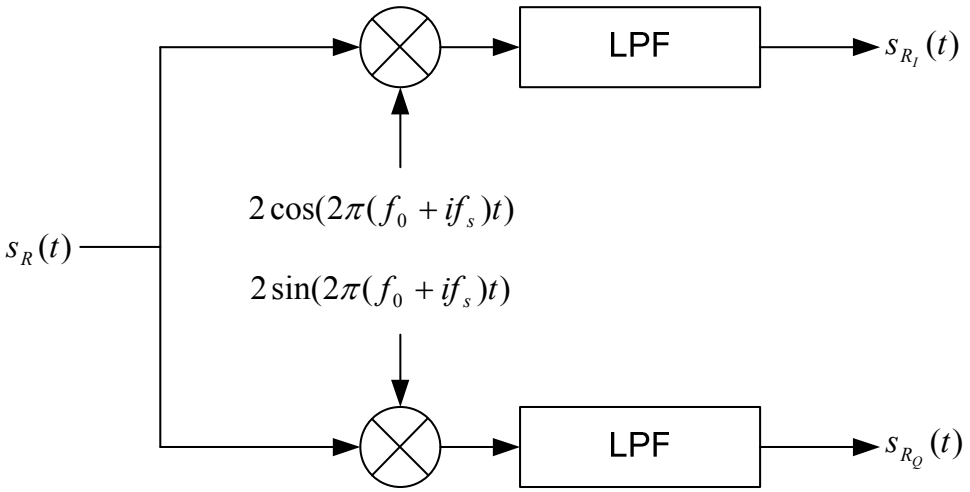

Figure 2.10: I-Q Demodulator.

The received signal is multiplied by the base band signal and low-pass filtered for obtaining the I-phase and Q-phase components. The obtained components can be expressed as follows,

$$s_{R_I}(t) = A\int_{-\infty-\infty}^{+\infty+\infty} g(x,y)\cos\left\{2\pi(f_0 + if_s)(t - \frac{2r}{c})\right\}2\cos(2\pi(f_0 + if_s)t)dxdy \tag{2.22}$$

$$s_{R_Q}(t) = A\int_{-\infty-\infty}^{+\infty+\infty} g(x,y)\cos\left\{2\pi(f_0 + if_s)(t - \frac{2r}{c})\right\}2\sin(2\pi(f_0 + if_s)t)dxdy \tag{2.23}$$

The output of the I-Q demodulator is combined for obtaining the raw radar data $s_{Raw}(t)$. This raw data is called the frequency signature of the target.

$$s_{Raw}(t) = s_{R_I}(t) + js_{R_Q}(t)$$

$$s_{Raw}(t) = A\int_{-\infty-\infty}^{+\infty+\infty} g(x,y)\exp\left\{ j2\pi(f_0 + if_s)\frac{2r}{c})\right\}dxdy \tag{2.24}$$

The range expression (2.12) can be put into (2.24) instead of r. Therefore, the received signal becomes [8][19],

$$s_{Raw}(t) = A\exp\left\{ j\frac{4\pi}{c}(f_0 + if_s)r_a\right\}\int_{-\infty-\infty}^{+\infty+\infty} g(x,y)\exp\left\{ j2\pi(f_0 + if_s)\frac{2(x\sin(wt) + y\cos(wt))}{c})\right\}dxdy$$

$$= A\exp\left\{ j\frac{4\pi}{c}(f_0 + if_s)r_a\right\}\int_{-\infty-\infty}^{+\infty+\infty} g(x,y)\exp\left\{- j2\pi(f_x x + f_y y)\right\}dxdy \tag{2.25}$$

where

$$f_x = -(f_0 + if_s)\frac{2\sin(wt)}{c} \tag{2.26}$$

and

$$f_y = -(f_0 + if_s)\frac{2\cos(wt)}{c} \tag{2.27}$$

There is an extraneous phase term in (2.25). The motion compensation algorithm compensates this phase term. (See Figure 2.11.) By tracking the range of the object during the imaging time, the phase term is vanished by multiplying both sides by the complex conjugate of it. Therefore, the resultant signal will be the 2D-Fourier transform of the reflectivity function of the target. The SF radar provides the samples of the 2D-Fourier transformation of the reflectivity function, $g(x,y)$, of the object.

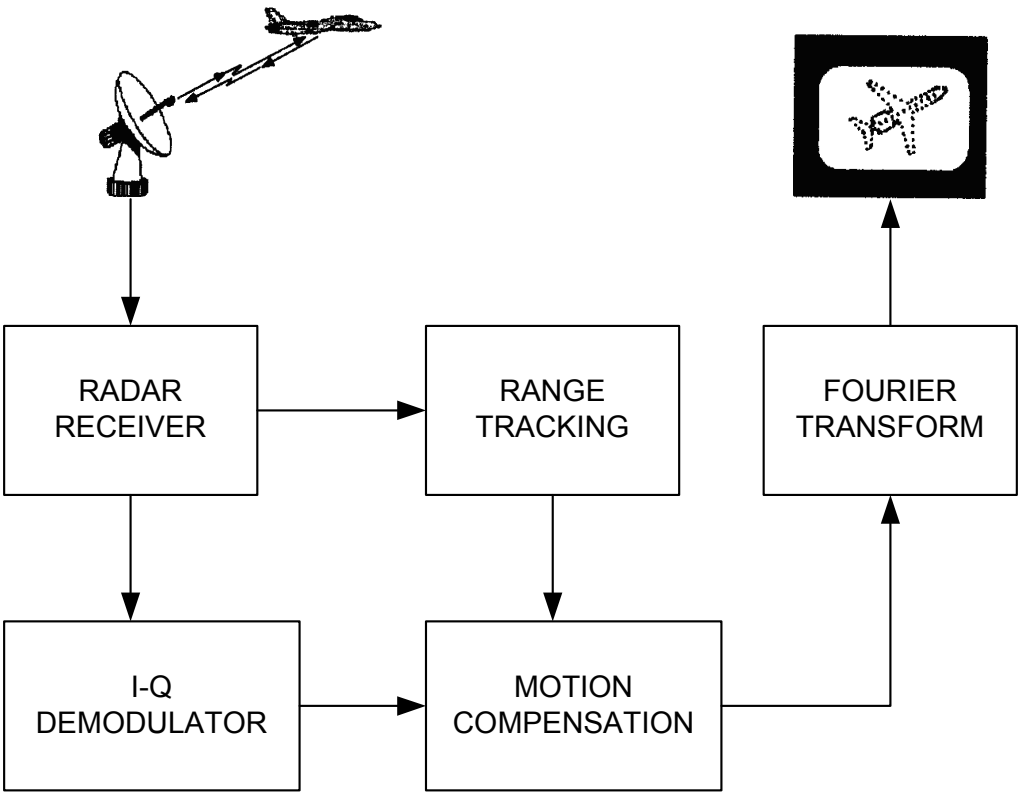

Figure 2.11: Conventional target imaging system.

CHAPTER 3

TARGET IMAGING
BY
JOINT TIME-FREQUENCY TRANSFORM

3.1 Introduction

Chapter 3 introduces the alternative way for suppressing the smearing and blurring effects on the target image. 2-D Fourier transform can yield reasonable results if the Doppler shift of the point scatterers on the target is not time-varying. Otherwise, sophisticated motion compensation algorithms should be used for obtaining clear images. In this chapter, the advantages of the JTFT techniques are investigated. The usage of the JTFT techniques for target imaging is explained and a proper JTFT, the Wigner-Ville Distribution and its properties are examined.

3.2 Use of Time-Frequency Transform for Target Imaging

Radar transmits electromagnetic wave and receives the reflected signal from the target. The image of the target is constructed over the range-cross range plane by using the reflected signal. The quality of the target image is determined by the resolution of the radar along the range and cross-range directions.

Since the target to be imaged can exhibit complex motions during the observation time, in most cases, the Doppler shift in received signal will not be time-invariant. Although the target exhibits a motion with constant rotation rate, the Doppler shift of the received signal will be time-varying [2][8][15]. Due to the relation between the cross-range resolution and the Doppler shift given in (2.16), the obtained image will be smeared along cross-range direction by the effect of time-varying Doppler shift [18][20]. Therefore, the conventional radar imaging method should use range tracking and Doppler tracking algorithms for using the Fourier transform properly.

Using a high resolution time-frequency transform instead of the Fourier transform for obtaining the Doppler shift information can make the Doppler tracking and complex motion compensation algorithms meaningless [8][11]. A time-frequency transform decomposes the signal into instantaneous time slices as shown in Figure 3.1. The magnitude of the time-frequency transform of a signal shows the distribution of the frequency content of the signal along the duration of the signal. On the other hand, the magnitude of the Fourier transform of the signal gives the frequency content of the signal but can not show any relation between time and frequency. The magnitude of the Fourier transform does not conduct how the frequency content of the signal changes with time.

The time-varying Doppler frequency shift can be treated as time-invariant in each time slice by using the time-frequency transform; hence the image smearing effect will be suppressed [6][12][18]. The Doppler frequency resolution, which determines the cross-range resolution, is determined by the resolution of the selected time-frequency transform technique. Figure 3.2 shows the basics of the target imaging by using the time-frequency analysis.

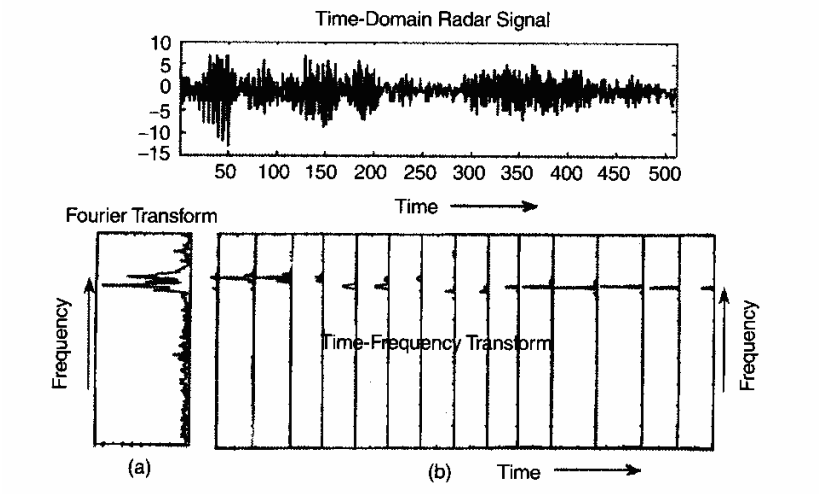

Figure 3.1: Time slicing of a signal.

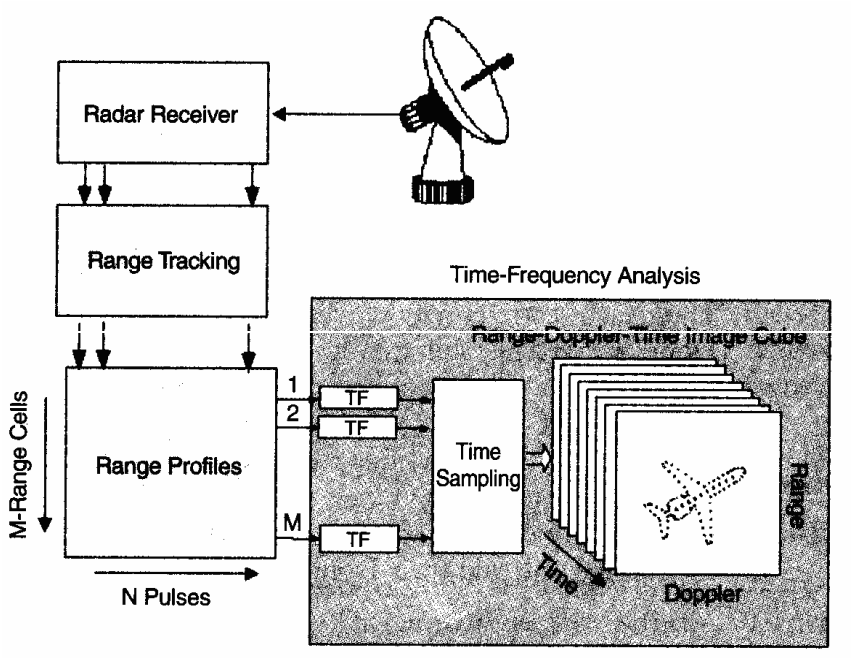

Figure 3.2: Target imaging system by Joint Time-Frequency Transform.

3.3 Data Acquisition from Step Frequency Modulated Radar

I-Q demodulated received signal is used to compose the MxN data matrix. (See Figure 3.3.) The received radar data in the form of MxN matrix is the target frequency signature. The data set contains M range profiles through N Doppler profiles [3][7].

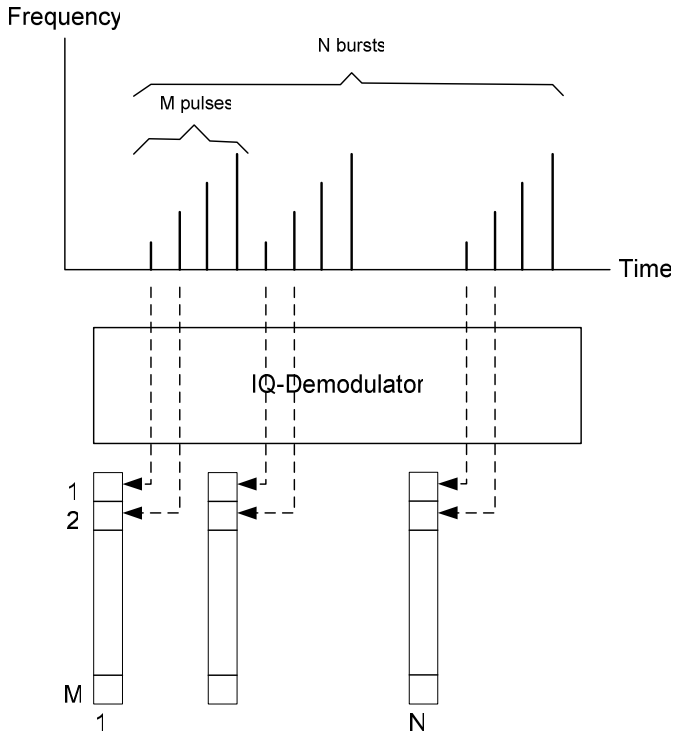

Figure 3.3: Data acquisition from the SF radar.

Taking the Fourier transform through the columns generates time history series of each range profile and ticks the locations of the point scatterers on the target along the range direction. The conventional target imaging method uses the Fourier

transform for obtaining the Doppler information in each range profile to differentiate the point scatterers along the cross-range direction [8].

Since the Doppler shift during observation time is time-varying in most cases, images obtained by the Fourier transform may suffer from smearing effect in the cross-range direction. The advantage of the JTFT over the Fourier transform can be used for obtaining time-varying Doppler information from the range profiles. By using a proper JTFT through each range cell creates image cube which contains the samples of image that can be constructed by the 2-D Fourier transform. (See Figure 3.4.) Although any time-frequency transform can give better results than the Fourier transform, selecting a high resolution JTFT technique in both time and frequency domains will bring advantages for the target imaging application.

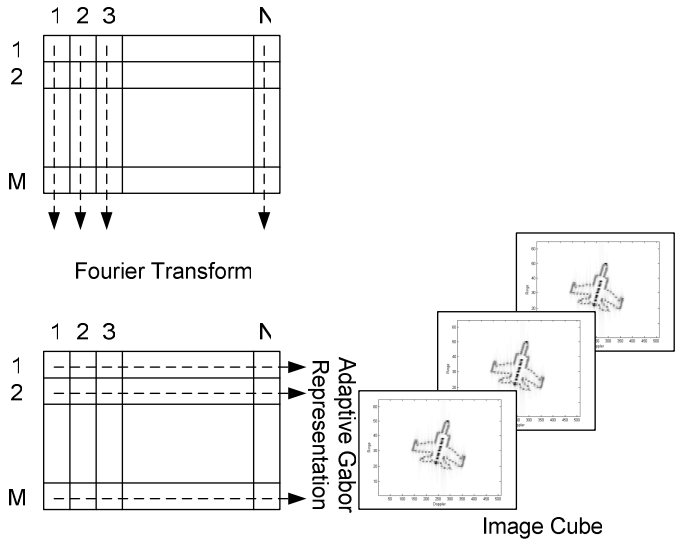

Figure 3.4: Application of JTFT on raw data.

3.4 Short Time Fourier Transform

The Short Time Fourier transform (STFT) can be one of the methods for target imaging by JTFT. The idea behind the STFT is very simple and useful. Suppose there is a signal which is composed of two different frequency sinusoidal signals, and suppose that the duration of the signal is about two minutes. When the Fourier transform of the signal is taken, the magnitude of the Fourier transform will show that there are two different frequency components in the signal but can not show the time information of the components. Duration of each component and the change of the frequency content of the signal can not be observed by the magnitude of the Fourier transform. The most straightforward thing to do is to break the signal, for example, into ten-second intervals and taking the Fourier transform of each interval. Therefore, the information about which frequency component is dominant in which time interval can be extracted from the analysis. The Fourier analysis of short duration parts can give an idea about how the frequency content of the signal is varying with time.

To study the properties of the signal at a given time instance, the signal should be emphasized at that time and the other part of the signal should be suppressed. This can be achieved by using a window function, $h(\tau - t)$, centered at time t. The modulated version, $s_t(\tau)$, of a given signal, $s(\tau)$, will be,

$$s_t(\tau) = s(\tau)h(\tau - t) \tag{3.1}$$

The modulated signal is function of two parameters, the fixed time, t, around which the properties of the signal will be investigated and the running time, τ. The window function is selected such that the original signal around t is

unaltered much, but it is suppressed at distant times from the time of interest. (See Figure 3.5.)

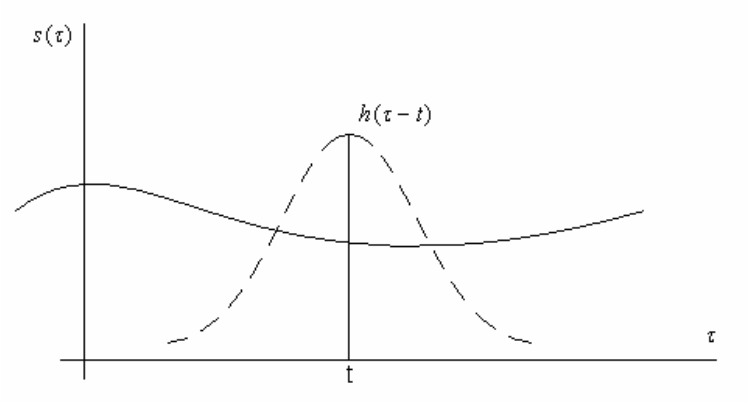

Figure 3.5 **:** Windowing the signal.

Since the modified signal extends around time t, taking the Fourier transform of the modulated signal will yield the distribution of frequency around that time.

$$S_t(w) = \int_{-\infty}^{+\infty} s(\tau)h(\tau - t)\exp(-jw\tau)d\tau \tag{3.2}$$

Since the modulated signal is short time form of the original signal, its Fourier transform will be the Short Time Fourier transform of the signal.

Resolution in time and frequency strictly depends on the shape of the selected window function in the STFT. The STFT expression, (3.2), can be interpreted as the similarity between the original signal and the time shifted window function. Therefore, the STFT tries to find the best representation for the original signal over the time-frequency plane, which is tiled by the resolution cell of the selected

window function [7]. The dimensions of the tiling windows over the time-frequency plane are determined by the window function and bounded by the uncertainty principle [9].

3.5 Optimum Window for Short Time Fourier Transform

Since there is a trade off between time and frequency resolutions, obtaining best resolutions in both domains at the same time is not possible; but finding an optimum window function which gives the best frequency resolution for pre-determined time resolution is possible [9].

Since the trade off between time and frequency resolution is controlled by the uncertainty principle, a window function which satisfies the uncertainty principle with equality is nothing but the optimum window function for STFT. A window function in the form of (3.3) with unit energy satisfies the uncertainty principle with equality [4][9].

$$\frac{d}{dt}h(t) = -kth(t) \tag{3.3}$$

A simple form for the window function which satisfies (3.3) can be given as,

$$h(t) = ce^{-\frac{k}{2}t^2} \tag{3.4}$$

where k is a positive constant, which controls the time variance of the window function.

Beside satisfying (3.3), there is another condition for the window function. The window function should be the unit energy signal,

$$E_h = \int_{-\infty}^{+\infty} |h(t)|^2 \, dt = 1$$

Therefore, the optimum window function for the STFT can be found as [4],

$$h(t) = \sqrt[4]{\frac{k}{\pi}} e^{-\frac{k}{2}t^2} \tag{3.5}$$

3.6 Wigner - Ville Distribution

According to the Wiener-Khinchin theorem, the power spectrum of a signal can be found by taking the Fourier transform of the auto-correlation function of the signal [4]. The auto-correlation function, $R(\tau)$, of the signal $s(t)$ is defined as,

$$R(\tau) = \int_{-\infty}^{+\infty} s(t) s^*(t-\tau) dt \tag{3.6}$$

The power spectrum of the signal can be represented by [4][9],

$$PS(w) = |S(w)|^2 = \int_{-\infty}^{+\infty} R(\tau) \exp(-jw\tau) d\tau \tag{3.7}$$

The relation between the frequency content of the signal and time can be constructed by using a time dependent auto-correlation function, $R(t,\tau)$,

$$PS(t,w) = \int_{-\infty}^{+\infty} R(t,\tau)\exp(-jw\tau)d\tau \tag{3.8}$$

Apparently the time dependent auto-correlation function can not be chosen arbitrarily. The time dependent power spectrum of the signal should give the power spectrum of the signal when integrated over time domain.

$$\int_{-\infty}^{+\infty} PS(t,w)dt = \left|S(w)\right|^2 \tag{3.9}$$

The condition given by (3.9) is known as frequency marginal condition [4][7]. Similarly, the integration of the time dependent power spectrum over the frequency plane should give the instantaneous power of the signal.

$$\frac{1}{2\pi}\int_{-\infty}^{+\infty} PS(t,w)dw = \left|s(t)\right|^2 \tag{3.10}$$

The constraint given by (3.10) is called the time marginal condition and since $PS(t,w)$ shows the power distribution over the time-frequency plane, the time dependent power spectrum should also be real and non-negative [4].

The Wigner-Ville Distribution uses the time dependent auto-correlation function chosen as [4][7][8],

$$R(t,\tau) = s(t+\frac{\tau}{2})s^*(t-\frac{\tau}{2}) \tag{3.11}$$

By using (3.11) in (3.8), the Wigner-Ville Distribution can be written as follows,

$$WVD_s(t,w) = \int_{-\infty}^{+\infty} s(t+\frac{\tau}{2}) s^*(t-\frac{\tau}{2}) \exp(-jw\tau) d\tau \tag{3.12}$$

(3.12) is called the auto-WVD [4]. By using the same naming convention, the cross-WVD is defined as,

$$WVD_{sg}(t,w) = \int_{-\infty}^{+\infty} s(t+\frac{\tau}{2}) g^*(t-\frac{\tau}{2}) \exp(-jw\tau) d\tau \tag{3.13}$$

The WVD satisfies the frequency and time marginal conditions given by (3.9**)** and (3.10) [4]. Beside satisfying the marginal conditions, the WVD is also a real valued function.

The WVD has also instantaneous frequency property, which shows the accuracy of the transform for observing the frequency content of a signal. The conditional mean frequency obtained by the WVD is equal to the mean frequency value at that time.

3.7 Wigner-Ville Distribution of the Sum of Signals

The main deficiency for WVD is the so-called cross-term interference. For example let the signal $s(t)$ be defined as,

$$s(t) = s_1(t) + s_2(t) \tag{3.14}$$

Therefore, the WVD of the defined signal above can be represented by using the cross-WVD definition given in (3.13),

$$WVD_s(t,w) = WVD_{s_1}(t,w) + WVD_{s_2}(t,w) + WVD_{s_1,s_2}(t,w) + WVD_{s_2,s_1}(t,w) \qquad (3.15)$$

Therefore, the WVD of signal $s(t)$ is found as,

$$WVD_s(t,w) = WVD_{s_1}(t,w) + WVD_{s_2}(t,w) + 2\,\mathrm{Re}\left\{WVD_{s_1,s_2}(t,w)\right\} \qquad (3.16)$$

(3.16) shows that the WVD of the sum of the signals is not the sum of the WVD of each signal. In addition to auto-terms, (3.16) also contains the cross-term. Since the magnitude of the cross-term is twice as large as the auto-terms, the cross-term usually destroys the useful information of the analysis [16].

The WVD can not be used directly in the target imaging due to cross-term interference. By using adaptive representation of the signal, the WVD can be turned into a useful tool for many applications.

CHAPTER 4

USING WIGNER-VILLE DISTRIBUTION FOR TARGET IMAGING

4.1 Introduction

Chapter 4 introduces the adaptive representation of a signal, which makes the WVD useful for spectral analysis. In adaptive representation, the Adaptive Gabor Representation is studied. Two search algorithms are introduced for implementation of the AGR, Coarse-to-Fine Search Algorithm and Matching Pursuit Search Algorithm. Also two new search algorithms are studied for obtaining better results in target imaging applications. The first one of the proposed algorithms is the Matching Pursuit with Reduced Dictionary and the second one is the Hybrid Matching Pursuit. The details of the implementations for the algorithms are explained through out Chapter 4.

4.2 Adaptive Representation

The usage of the Wigner-Ville Distribution can be possible if the cross-term interference is reduced or totally suppressed [8]. One of the methods for getting out of the cross term interference is adaptive representation of the signal [11].

For decomposing the signal by adaptive representation, the elementary functions are used. The signal, $s(t)$, can be synthesized by using elementary functions, $h_p(t)$, as follows,

$$s(t) = \sum_p B_p h_p(t) \tag{4.1}$$

where B_p is a constant and stands for the similarity between the corresponding elementary function and the signal that is to be analyzed.

B_p can be found by using the inner product,

$$B_p = \left\langle s(t), h_p(t) \right\rangle \tag{4.2}$$

Since the elementary function will contain three parameters for time center, frequency center and time width, trying to find an analytical solution for the best elementary function may not be feasible. Therefore, an iterative approach can be used for finding the best representation of the signal [11][17].

For $p = 0$, the initial signal, $s_0(t)$ is taken as the signal itself, $s_0(t) = s(t)$. The first elementary function, $h_0(t)$, and the corresponding constant coefficient, B_o, is found as follows,

$$\left|B_o\right|^2 = \max_{h_0} \left|\left\langle s_0(t), h_0(t) \right\rangle\right|^2$$

This is nothing but the maximization problem for finding the most similar elementary function to $s_0(t)$. The elementary function, $h_0(t)$, which maximizes the inner product term gives the desired coefficient B_o.

After the first coefficient is found, the iteration goes on with the remainder signal, $s_1(t)$, that can be found by,

$$s_1(t) = s_0(t) - B_0 h_0(t)$$

The general form of the equations at the p-th step of the iteration can be represented as follows [11],

$$\left|B_p\right|^2 = \max_{h_p} \left|\left\langle s_p(t), h_p(t) \right\rangle\right|^2 \tag{4.3}$$

$$s_{p+1}(t) = s_p(t) - B_p h_p(t) \tag{4.4}$$

Without loss of generality, the energy of the elementary function can be taken as unity,

$$\left\|h_p(t)\right\|^2 = \int_{-\infty}^{+\infty} \left|h_p(t)\right|^2 dt = 1 \tag{4.5}$$

then the energy of the residual signal is,

$$\left\|s_{p+1}(t)\right\|^2 = \left\|s_p(t)\right\|^2 - \left|B_p\right|^2 \tag{4.6}$$

The following vector representation shows the idea of the iteration method.

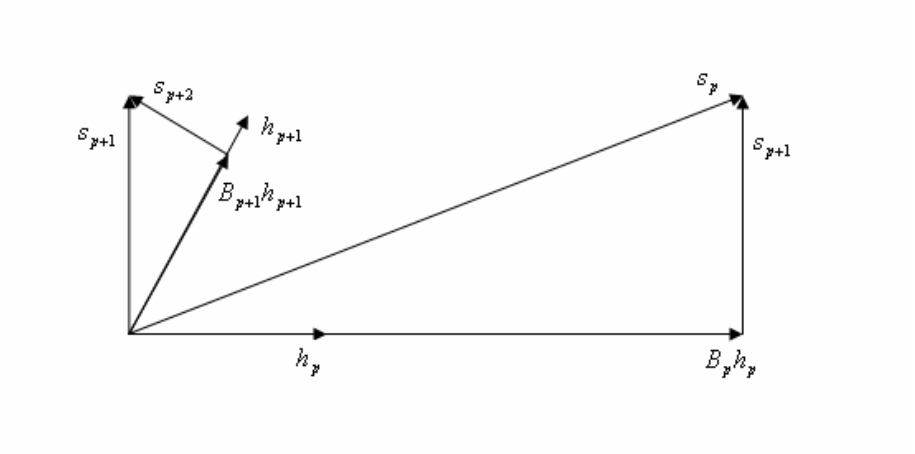

Figure 4.1: Vector representation of the iteration method.

The quality of the adaptive representation of the signal depends on the energy of the residual signal. If the energy of the residual signal approaches to zero, the representation decomposes the signal successfully.

Let the angle between the signal $s_p(t)$ and $B_p h_p(t)$ be θ_p. From Figure 4.1,

$$\cos(\theta_p) = \frac{B_p}{\|s_p(t)\|} = \frac{\langle s_p, h_p \rangle}{\|s_p(t)\|}$$

Therefore,

$$B_p = \cos(\theta_p)\|s_p(t)\| \tag{4.7}$$

By using (4.7) in the energy expression of residual signal given by (4.6), the residual energy can be expressed by [10][11],

$$\left\|s_{p+1}(t)\right\|^2 = \left\|s_p(t)\right\|^2 \sin^2(\theta_p) \tag{4.8}$$

Then,

$$\left\|s_1(t)\right\|^2 = \left\|s_0(t)\right\|^2 \sin^2(\theta_0)$$

$$\left\|s_2(t)\right\|^2 = \left\|s_1(t)\right\|^2 \sin^2(\theta_1)$$

….

$$\left\|s_p(t)\right\|^2 = \left\|s_{p-1}(t)\right\|^2 \sin^2(\theta_{p-1})$$

and hence,

$$\left\|s_p(t)\right\|^2 = \left\|s_0(t)\right\|^2 \prod_{i=0}^{p-1} \sin^2(\theta_i) \tag{4.9}$$

Therefore, the residual signal energy at step p can be represented by using the energy of the signal to be decomposed. (4.9) can be turned into a simple inequality as follows,

$$\left\|s_p(t)\right\|^2 = \left\|s_0(t)\right\|^2 \prod_{i=0}^{p-1} \sin^2(\theta_i) \le \left\|s_0(t)\right\|^2 \left(\sin(\theta_{\max})\right)^{2p} \tag{4.10}$$

where $\sin(\theta_{\max}) = \max_{\theta_p}\left(\sin(\theta_p)\right)$.

Assuming that there always exists an elementary function, $h_p(t)$ that is not perpendicular to $s_p(t)$ [11],

$$\left\|s_p(t)\right\|^2 \le \left\|s_0(t)\right\|^2 \left(\sin(\theta_{\max})\right)^{2p} \to 0 \text{ as } p \to \infty \tag{4.11}$$

(4.11) shows that a signal $s(t)$ can be represented exactly by using infinite number of elementary functions.

Since the used elementary function is parameterized, the set of elementary functions found for representation of a signal may not be the same for another signal. The elementary functions show differences according to the selected signal, even the energy of residual signal approaches to zero.

4.3 Adaptive Spectrogram

A signal, $s(t)$, can be decomposed into elementary functions as shown in (4.1). Therefore, the Wigner-Ville Distribution of the signal can be written as [9],

$$WVD_{s(t)}(t,w) = WVD\left(\sum_p B_p h_p(t)\right) \tag{4.12}$$

(4.12) shows the energy distribution of the signal on the time-frequency plane since the Wigner-Ville Distribution satisfies the time and frequency marginal conditions. In other words,

$$\frac{1}{2\pi}\int_{-\infty}^{+\infty}\int_{-\infty}^{+\infty} WVD_{s(t)}(t,w)dwdt = \left\|s(t)\right\|^2 \tag{4.13}$$

The energy of the signal, $s(t)$, can be expressed by using the residual signal energy equation given by (4.6) [4],

$$\left\|s(t)\right\|^2 = \sum_p \left|B_p\right|^2 \tag{4.14}$$

(4.14) is the energy conservation equation and is similar to Parseval's relation in the Fourier transform.

The WVD of the signal can be put into summation of the WVD of auto-terms and the WVD of cross-terms by using the adaptive representation of the signal as follows,

$$WVD_s(t,w) = \sum_p B_p^2 WVD_{h_p}(t,w) + \sum_{p\neq q} B_p B_q^* WVD_{h_p h_q}(t,w) \tag{4.15}$$

The first term in (4.15) stands for auto terms and the second term stands for cross terms. Since,

$$\frac{1}{2\pi}\int_{-\infty-\infty}^{+\infty+\infty} WVD_{h_p}(t,w)dwdt = \left\|h_p(t)\right\|^2 = 1$$

then,

$$\frac{1}{2\pi}\int_{-\infty-\infty}^{+\infty+\infty} WVD_s(t,w)dwdt = \sum_p B_p^2 + \frac{1}{2\pi}\int_{-\infty-\infty}^{+\infty+\infty}\sum_{p\neq q} B_p B_q^* WVD_{h_p h_q}(t,w)dtdw \tag{4.16}$$

By using (4.13) and (4.14),

$$\frac{1}{2\pi}\int_{-\infty-\infty}^{+\infty+\infty}\sum_{p\neq q} B_p B_q^* WVD_{h_p h_q}(t,w)dtdw = 0 \tag{4.17}$$

(4.17) implies that the cross-term energy in (4.15) is equal to zero. Therefore, a new time-dependent representation can be defined as follows [4][17],

$$AS(t,w) = \sum_p \left|B_p\right|^2 WVD_{h_p}(t,w) \tag{4.18}$$

Because it is an adaptive representation based time-dependent spectrum, (4.18) is called the adaptive spectrogram (AS). The adaptive spectrogram uses the Wigner-Ville Distribution but does not contain any cross-term interference. It also satisfies the energy conservation relation similar to the Wigner-Ville Distribution.

$$\left\|s(t)\right\|^2 = \frac{1}{2\pi}\int_{-\infty-\infty}^{+\infty+\infty}\sum_p \left|B_p\right|^2 WVD_{h_p}(t,w) = \frac{1}{2\pi}\int_{-\infty-\infty}^{+\infty+\infty} AS(t,w)dtdw \tag{4.19}$$

As mentioned before, the fundamental issue of adaptive representation is to find the elementary functions for the signal to be decomposed. The adaptive representation process starts with a parametric model for the elementary function and the signal processing time for the representation increases with the better matching quality.

The adaptive representation and the adaptive spectrogram are independent of the selection of the elementary function. Any type of function can be used as elementary function for both of the processes. Selecting the elementary function that has a good time and frequency resolution brings advantages together.

4.4 Adaptive Gabor Representation

In principle, the elementary function can be selected in any form. Selecting the localized functions in the time and frequency domain helps better representation of the signal. The Gaussian type window function satisfies the uncertainty inequality with equality, and the adaptive representation with Gaussian type elementary function is called the Adaptive Gabor Representation (AGR).

The selected elementary function form, $h_p(t)$, is the time shifted and frequency modulated version of the Gaussian function [10][11].

$$h_p(t) = \sqrt[4]{\frac{\alpha_p}{\pi}} \exp\left\{-\frac{\alpha_p}{2}(t-T_p)^2\right\} \exp\{jW_p t\} \tag{4.20}$$

where (T_p, W_p) is the time and frequency center of the elementary function and $1/2\alpha_p$ is the time variance of the elementary function. The role of α_p is important for the time and frequency resolution of the elementary function. (See Figure 4.2.)

In the adaptive representation, the variance of the elementary function is adjustable. The time and frequency centers of the elementary function are not fixed. Adjusting the variance changes the duration of the elementary function, and adjusting the parameters (T_p, W_p) change the localization center. Changing the variance and the time-frequency center of the elementary function makes possible to represent the time and frequency behaviors locally.

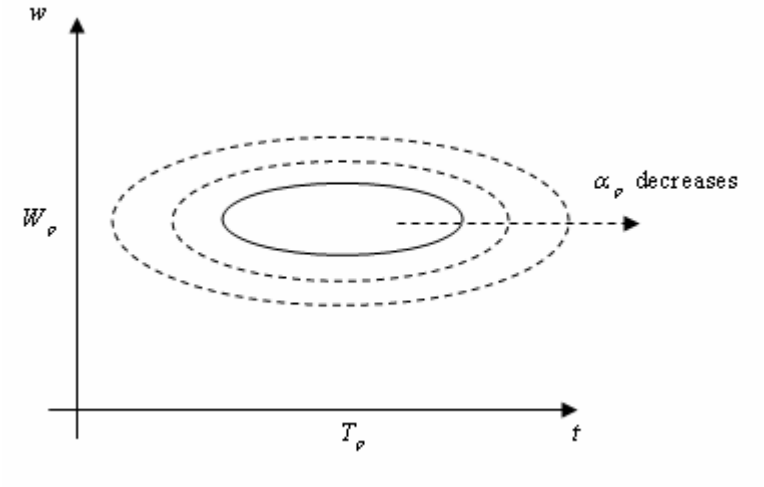

Figure 4.2: Change of time-frequency resolution with α_p.

The WVD of the time shifted and frequency modulated version of the Gaussian function given in (4.20) is,

$$WVD_{h_p}(t,w) = 2\exp\left\{-\alpha_p(t-T_p)^2 - \frac{(w-W_p)^2}{\alpha_p}\right\} \tag{4.21}$$

By using the Gaussian function in adaptive representation given in (4.20), the adaptive spectrogram in (4.18) becomes [4],

$$AS(t,w) = 2\sum_p \left|B_p\right|^2 \exp\left\{-\alpha_p(t-T_p)^2 - \frac{(w-W_p)^2}{\alpha_p}\right\} \tag{4.22}$$

Since the time and frequency resolution of the Gaussian function is determined by the variance, the computations of the optimal h_p become rather simple.

4.5 Implementation of the Adaptive Gabor Representation

In fact, the adaptive time-frequency transform is computed by a number of orthogonal projections of the signal on to the elementary Gaussian functions. By assuming that the best elementary functions are found, somehow, the main steps for the implementation of the AGR can be summarized as follows.

Step 1 : Given a signal to be analyzed, $s(t)$, at stage $p = 0$ with $s_0(t) = s_{p=0}(t) = s(t)$, find an elementary function $h_0(t) = h_{p=0}(t)$ by adjusting the parameters $(T_{p=0}, W_{p=0}, \alpha_{p=0})$ such that $h_0(t)$ is the most similar elementary function to $s_0(t)$.

Step 2: Compute the orthogonal projection, B_0, of $s_0(t)$ onto $h_0(t)$ and the remainder signal, $s_1(t) = s_0(t) - B_0 h_0(t)$.

Step 3 : Use the remainder $s_1(t)$ to find the next optimal elementary function, $h_1(t) = h_{p=1}(t)$.

Step 4 : Repeat the procedure described above until the norm of the remainder signal, $\|s_{p+1}(t)\|$, is less than a predetermined limit.

4.6 Coarse-to-Fine Search Algorithm

The most important point in adaptive time-frequency representation is to find the optimal parameters for the Gaussian elementary functions. At each step of the

iteration, the found Gaussian elementary function should be the most similar one to the remainder signal. Thus, at step p, the projection of $s_p(t)$ onto $h_p(t)$ becomes a maximization problem given by,

$$\left|B_p\right|^2 = \max_{T_p,W_p,\alpha_p}\left|\int_{-\infty}^{+\infty} s_p(t)h_p^*(t)dt\right|^2 \tag{4.23}$$

The solution of (4.23) is the major problem in the adaptive representation. Instead of finding an analytical solution, an iterative method which is called the Coarse-to-Fine Search Algorithm is applied to find the best Gaussian elementary function [11].

The algorithm is based on the inner product given below,

$$\begin{aligned}\Gamma_{T_p,W_p,\alpha_p} &= \int_{-\infty}^{+\infty} s_p(t)h_p^*(t)dt \\ &= \sqrt[4]{\frac{\alpha_p}{\pi}}\int_{-\infty}^{+\infty} s_p(t)\exp\left\{-\frac{\alpha_p}{2}(t-T_p)^2\right\}\exp\{-jW_p t\}dt\end{aligned} \tag{4.24}$$

Since the selected elementary function is the time shifted and frequency modulated Gaussian function, (4.24) is nothing but the Fourier transform of the product $s_p(t)\exp\left\{-\frac{\alpha_p}{2}(t-T_p)^2\right\}$. This gives an opportunity for performing an effective searching algorithm for finding the maximum Γ. Once the parameters T_p and α_p are selected, finding the optimal W_p turns into choosing the largest Fourier transform coefficient in magnitude, and the found coefficient will point out the frequency center, W_p, of the elementary function.

The algorithm starts with an assumed value of α_p. After selecting the time variance, the time center of the Gabor function, T_p, is changed through out the duration of the signal and the Fourier transform of the product, $s_p(t)\exp\left\{-\frac{\alpha_p}{2}(t-T_p)^2\right\}$, is calculated for each value of T_p until finding the largest magnitude Fourier transform coefficient.

Since there is a close relation between α_p and time variance of the elementary function, at each step, the value of α_p is increased by a predetermined manner so that the time variance of the elementary Gabor function is decreased gradually for fine search of the time center T_p. (See Figure 4.3.)

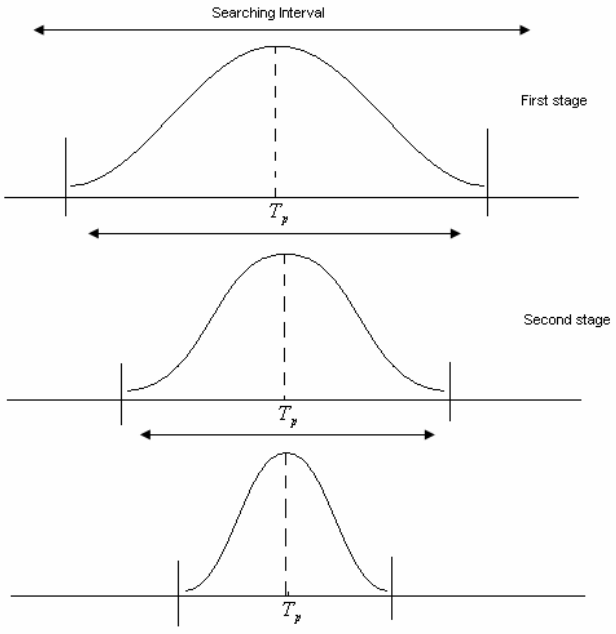

Figure 4.3: Searching interval of the Coarse-to-Fine Search Algorithm.

4.7 Matching Pursuit Algorithm

The AGR is one of the efficient methods for utilizing the Wigner-Ville Distribution in the AS. The main problem in the AGR is to find the best elementary Gabor function. One of the proposed methods for searching the best elementary function is the Coarse-to-Fine Search Algorithm. The Matching Pursuit Algorithm can be another alternative method for implementing the AGR.

In the MP Algorithm, the possible elementary functions are predetermined and the searching algorithm is run over the collection of the selected elementary function set which is called the function dictionary. Since the dimension of the set is finite, the searching time for best elementary function can be reduced drastically. The number of inner product operation to be performed is also reduced by using the MP Algorithm.

In the MP Algorithm, the selected dictionary is a redundant set of elementary functions. Therefore, the number of elementary functions in the set can be too large, but finite. Despite this drawback, the MP Algorithm can decompose a signal faster than the Coarse-to-Fine Search Algorithm.

To explain the MP Algorithm, let us assume that the dictionary of the elementary functions, Ψ, contains N elements,

$$\Psi = \left\{h_1(t), h_2(t), ...h_p(t), ...h_{N-1}(t), h_N(t)\right\}$$

where $h_p(t)$ is given in (4.20).

After constructing the dictionary, the MP Algorithm can be explained by showing the decomposition of the signal $s(t) = s_0(t)$.

Step 1 : Calculate the inner product of the signal $s(t)$ with the elements of the dictionary, and store the values into 1xN matrix, $\Gamma_{s_0 h}$.

$$\Gamma_{s_0 h} = \left[\langle s(t), h_1(t) \rangle \quad \langle s(t), h_2(t) \rangle \quad \ldots \quad \langle s(t), h_p(t) \rangle \quad \ldots \quad \langle s(t), h_N(t) \rangle \right]$$

Step 2 : Calculate the inner product of each element in the dictionary with the other elements of the dictionary, and store the values into NxN matrix, Γ_{hh}.

$$\Gamma_{hh} = \begin{bmatrix} \langle h_1(t), h_1(t) \rangle & \langle h_1(t), h_2(t) \rangle & .. & \langle h_1(t), h_p(t) \rangle & .. & \langle h_1(t), h_N(t) \rangle \\ \langle h_2(t), h_1(t) \rangle & \langle h_2(t), h_2(t) \rangle & .. & \langle h_2(t), h_p(t) \rangle & .. & \langle h_2(t), h_N(t) \rangle \\ \vdots & \vdots & & \vdots & & \vdots \\ \langle h_p(t), h_1(t) \rangle & \langle h_p(t), h_2(t) \rangle & .. & \langle h_p(t), h_p(t) \rangle & .. & \langle h_p(t), h_N(t) \rangle \\ \vdots & \vdots & & \vdots & & \vdots \\ \langle h_N(t), h_1(t) \rangle & \langle h_N(t), h_2(t) \rangle & .. & \langle h_N(t), h_p(t) \rangle & .. & \langle h_N(t), h_N(t) \rangle \end{bmatrix}$$

Step 3 : Find the greatest entry of $\Gamma_{s_0 h}$ in magnitude to determine B_0 and the corresponding best matching elementary function, $h_p(t)$, in the dictionary.

Step 4 : Calculate the inner product of the next remainder signal, $s_1(t)$, with the dictionary functions by using the following equation obtained from (4.4).

$$\Gamma_{s_1 h} = \Gamma_{s_o h} - B_0 \Gamma_{hh}(p) \tag{4.25}$$

where $\Gamma_{hh}(p)$ is the p-th row of Γ_{hh}.

Step 5 : If the iteration limit is not reached, continue with step 3 to find the next elementary function by using $\Gamma_{s_1 h}$.

As seen from the algorithm steps, the most complex operation is finding the maximum element in magnitude from a 1xN matrix. After calculating the necessary inner products in step 1 and step 2, each of the remaining iterations may take processing time as much as the FFT operation takes.

4.8 Matching Pursuit Algorithm with Reduced Dictionary

The dictionary for the MP Algorithm is composed by sweeping three parameters in the Gabor elementary function with constant step lengths. The step lengths of the parameters are determined by the number of points taken from the signal, as indicated in [17].

Although the idea behind the MP Algorithm is very effective, the dimension of the constructed dictionary introduces a new deficiency for the algorithm. Since the dimension of the dictionary depends on the number of samples taken from the signal, management of the dictionary is a challenging work, even for a 256-point signal. The memory requirement of the MP Algorithm will drastically increase by increasing the number of samples taken from the signal. (See Table 4.1.) (The memory requirements are approximate and calculated by MATLAB.)

The proposed method, the MP with Reduced Dictionary (MP-RD), makes the MP Algorithm feasible for the signal decomposition. The memory requirement of the algorithm is reduced by decreasing the dimension of the function dictionary. The reduction in the dimension of the dictionary causes the decrease in the frequency

resolution, but the application of the MP Algorithm for a 512-point signal is made possible. (See Table 4.2.)

Table 4.1 : The dictionary dimensions for the MP Algorithm.

NUMBER OF SAMPLES	DICTIONARY DIMENSION	MEMORY (MByte)
64	1597	42.07
128	3710	224.60
256	8447	1154.93
512	18944	5772.43

Table 4.2 : The dictionary dimensions for the MP-RD Algorithm.

NUMBER OF SAMPLES	SIMILARITY COEFFICIENT	DICTIONARY DIMENSION	MEMORY (MByte)
256	0.50	713	13.34
256	0.80	1531	47.76
512	0.75	2768	160.22
512	0.80	3529	245.25
512	0.85	4079	317.70

The candidate dictionary functions are determined according to the attitude given in [17], but the functions which satisfy the selection criteria are appended to the dictionary. By using proper selection criteria, similar elementary functions are eliminated from the dictionary.

The inner product operation is used for determining the similarity between two elementary functions, and the amount of similarity is limited by a similarity

coefficient, δ_S. For example, whether the elementary function $h_m(t)$ is similar to $h_n(t)$ or not is determined by investigating the following inequality.

$$\left\|\left\langle h_m(t), h_n(t)\right\rangle\right\| \le \delta_S \left\|h_n(t)\right\|^2 \tag{4.26}$$

If the inequality given by (4.26) is not satisfied, the elementary function, $h_m(t)$, is assumed as similar to $h_n(t)$ and is not appended to the dictionary.

The only difference between the MP-RD Algorithm and the MP Algorithm is just the used function dictionary. The construction of the dictionary for the MP-RD Algorithm can be explained in 5 steps, as follows.

Step 1 : Determine the similarity coefficient for the dictionary.

Step 2 : Pick up the first elementary function as described in [17] and append it to the dictionary.

Step 3 : Pick up the candidate elementary function.

Step 4 : Check for the similarity of the candidate elementary function with all elements of the dictionary by using (4.26). If not similar, append it to the dictionary.

Step 5 : If not end, return to step 3.

By using the procedure described for the MP-RD Algorithm, the memory requirements of the MP Algorithm is reduced to a feasible level and so the processing time.

4.9 Hybrid Matching Pursuit Algorithm

The MP-RD Algorithm makes the MP Algorithm applicable by reducing the function dictionary dimension. Besides its advantages, the MP-RD Algorithm also reduces the frequency resolution with the dictionary dimension. Since the frequency resolution is reduced, the Doppler resolution of the target image is also reduced and the obtained image by the MP-RD Algorithm will show smearing through the cross-range direction.

On the other hand, the AGR with the CFS Algorithm has better resolution and the target images obtained by the CFS Algorithm are almost free of smearing effect. Therefore, another new approach is studied for suppressing the smearing effect on the target images obtained by the MP-RD Algorithm. The proposed new method tries to combine elite sides of the CFS Algorithm and the MP-RD Algorithm and will be called the Hybrid MP Algorithm.

By the Hybrid MP Algorithm the speed of the MP-RD Algorithm and the frequency resolution quality of the CFS Algorithm are tried to be combined. The CFS Algorithm spends much of the processing time for representing the high-frequency components of the signal. The sharp changes in the signal increase the number of iterations of the CFS Algorithm for decomposing the signal. However, the low frequency components of the signal are well represented on the time-frequency plane. On the other side, the MP-RD Algorithm can perform the same number of iterations in a shorter time than the CFS Algorithm.

Since the CFS Algorithm starts the decomposition with wide Gaussian elementary function, the low frequency components of the signal are decomposed first. After

a few iterations the remaining part from the signal is details and contains the high frequency components of the signal.

For better understanding the behavior of the CFS Algorithm, a sample signal, $s(t)$, is decomposed by the AGR with the CFS Algorithm;

$$s(t) = \exp(j2\pi f_1 t) + \exp(j2\pi f_2 t) + 3\delta(t - 0.0061) + 3\delta(t - 0.0119)$$

where $f_1 = 500Hz$ and $f_2 = 1000Hz$.

Figure 4.4 shows the magnitude of the selected input signal, and Figure 4.5 (a)-(d) show the magnitude of the remainder signal after 3, 5, 7 and 9 iterations of the algorithm, respectively.

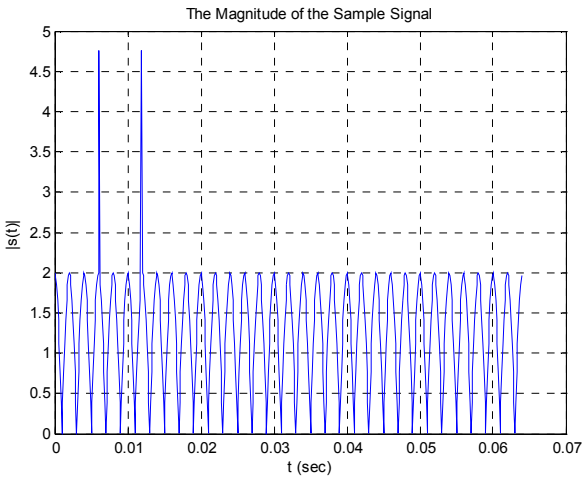

Figure 4.4: Magnitude of $s(t)$.

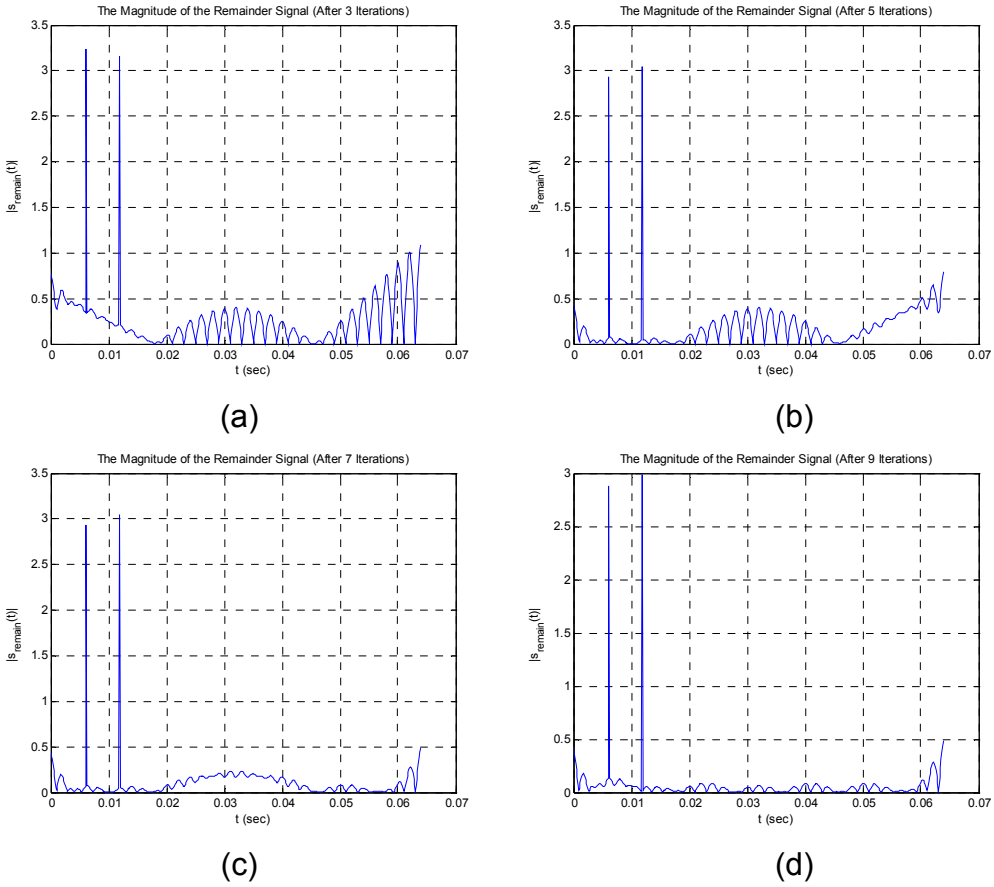

Figure 4.5: The magnitudes of the remainder signals.

Hence the procedure for the Hybrid MP Algorithm is constructed as follows.

Step 1 : Determine the number of iterations for the CFS Algorithm and the iteration limit.

Step 2 : Run the CFS Algorithm as many times as the number of iterations for the CFS Algorithm.

Step 3 : Pass the remainder signal to the MP-RD Algorithm and compute the new remainder signal.

Step 4 : Calculate the energy of the remainder signal and check for the iteration limit. If the limit is not reached, go on with step 3.

The number of iterations for the CFS Algorithm does not need to be a large number. Even three iterations can give acceptable results. By the Hybrid MP, the time consuming part for the CFS Algorithm is computed by the MP-RD Algorithm. Therefore, the desired resolution for the representation of the signal is obtained in a shorter time than the CFS Algorithm.

CHAPTER 5

APPLICATIONS OF THE METHODS

5.1 Introduction

Chapter 5 includes the applications of the searching methods. The methods are tried on the selected sample signals, and the results are presented for the comparison. Also the methods are used on the target imaging system by using the raw data of the simulated aircraft and the raw data of the MIG-25 aircraft obtained from http://airborne.nrl.navy.mil/~vchen/data.

5.2 Time-Frequency Analysis of Example Signals

The AGR is one of the methods for using the WVD in spectral analysis of signals [16]. By means of the AGR, the WVD, free of cross-term interference, can be applied. Chapter 4 suggested some methods for using the AGR in decomposition of signals. For observing the performances of the methods, the selected sample signals are decomposed by using the AGR and the signals are mapped onto the time-frequency plane.

The selected sample signals, $s_1(t), s_2(t), s_3(t)$, are given as follows.

$$s_1(t) = \sin(2\pi f_{11} t) + \sin(2\pi f_{12} t) + \sin(2\pi f_{13} t)$$

where $f_{11} = 1\,KHz$, $f_{12} = 2.7\,KHz$ and $f_{13} = 7.5\,KHz$.

$$s_2(t) = \sin(2\pi f_{21} t) + \sin(2\pi f_{22} t) + \delta(t - 0.0020) + \delta(t - 0.0040)$$

where $f_{21} = 1\,KHz$, $f_{22} = 7.7\,KHz$.

$$s_3(t) = \delta(t - 0.0020) + \delta(t - 0.0036)$$

The sample signals are sampled at the rate $25\,Ksamp/\sec$ and a total of 128 samples are considered.

$s_1(t)$ contains purely sinusoidal components. The frequencies of the components are selected as non-harmonic pairs. (See Figure 5.1 (a).) In $s_2(t)$, the sample signal is changed by adding two impulses with different hit times to the purely sinusoidal components. (See Figure 5.1 (b).) Therefore, the effect of sharp changes in the sinusoidal components is tried to be observed. The third sample signal, $s_3(t)$, contains only two impulses and used for obtaining an idea about the time and frequency resolution qualities of the methods. (See Figure 5.1 (c).)

The CFS, the MP, the MP-RD and the Hybrid MP search methods for the AGR are examined by using the given example signals. All of the searching algorithms are iterated until the energy of the remainder signal is less than or equal to (1/100) of the energy of the original signal. For the MP-RD and the Hybrid MP

Algorithms, the function dictionary is constructed by taking the similarity coefficient as 0.85, and the number of iterations of the CFS Algorithm in the Hybrid MP Algorithm is taken as 3.

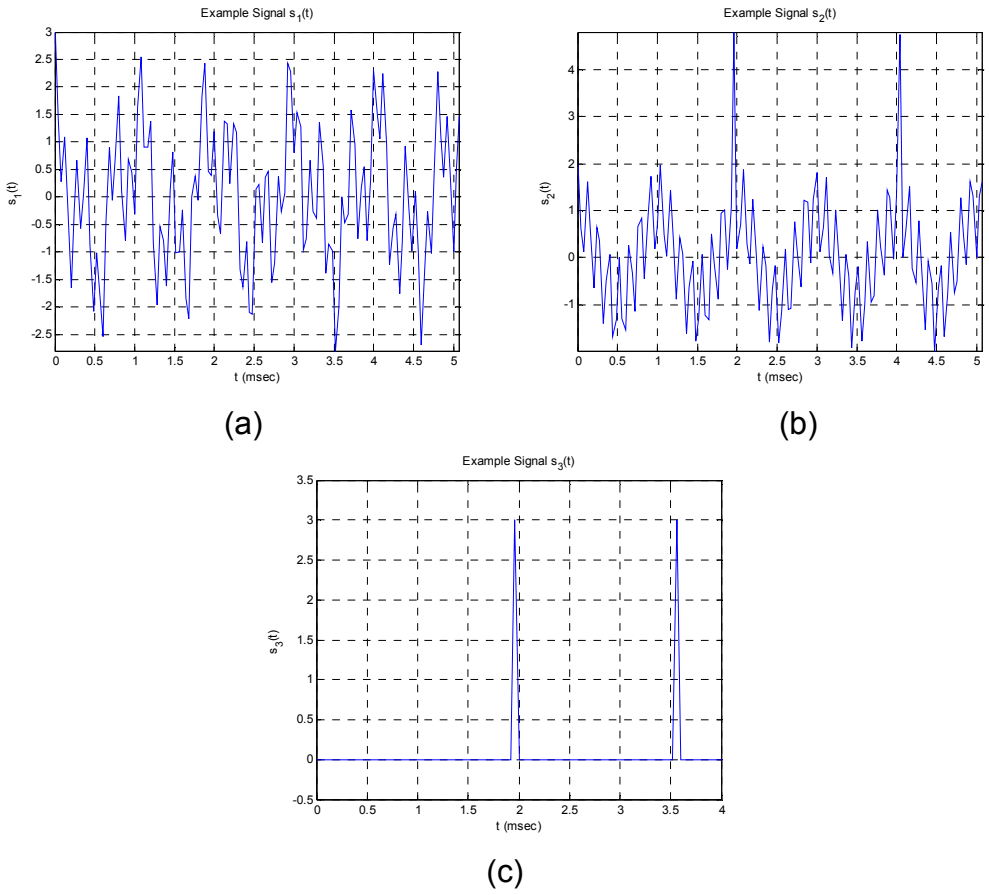

Figure 5.1 : The example signals for the AGR

Figure 5.2 to Figure 5.4 show the time-frequency plots of the sample signals and Figure 5.5 to Figure 5.7 show the graphs of the energy of the remainder signal versus the number of iterations performed. Table 5.1 gives the signal processing times in seconds for each of the searching algorithms.

Table 5.1 : Signal processing times of the algorithms in seconds.

	SEARCH ALGORITHM FOR THE AGR			
	CFS	MP	MP-RD	Hybrid-MP
$s_1(t)$	0.062	0.047	0.016	0.047
$s_2(t)$	0.109	0.063	0.016	0.047
$s_3(t)$	0.125	0.063	0.015	0.063

The signal processing time is reduced by the help of the MP Algorithm but, the representation quality of the AGR with the CFS can not be reached by other searching methods. By using the MP the signal processing time is almost pull down to half and the resolution of the representation is sacrificed much. The MP-RD method reduced the processing time more and the obtained resolution is not worse than the MP Algorithm. If the loss of resolution is not much critical, the usage of MP Algorithm can be a logical choice for the AGR instead of the CFS or the MP. On the other hand, the Hybrid MP Algorithm helps the MP-RD Algorithm for the time-frequency resolution of the representation. The results obtained by the Hybrid MP Algorithm are very close to those of the CFS Algorithm; the processing time of the Hybrid MP can be as long as the processing time of the CFS, but the less memory requirement of the Hybrid MP is the main advantage. Hence the MP-RD and the Hybrid MP methods can be good candidates for making the AGR useful in target imaging systems.

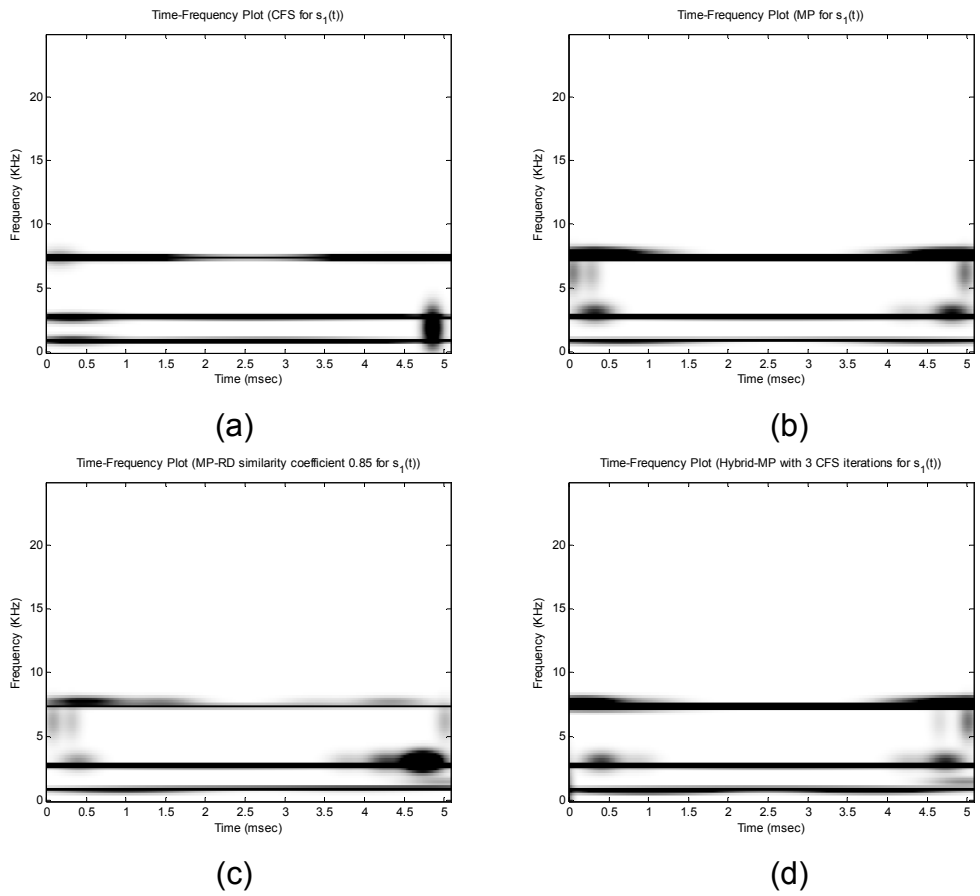

Figure 5.2 : Time-Frequency plots of the sample signal $s_1(t)$.

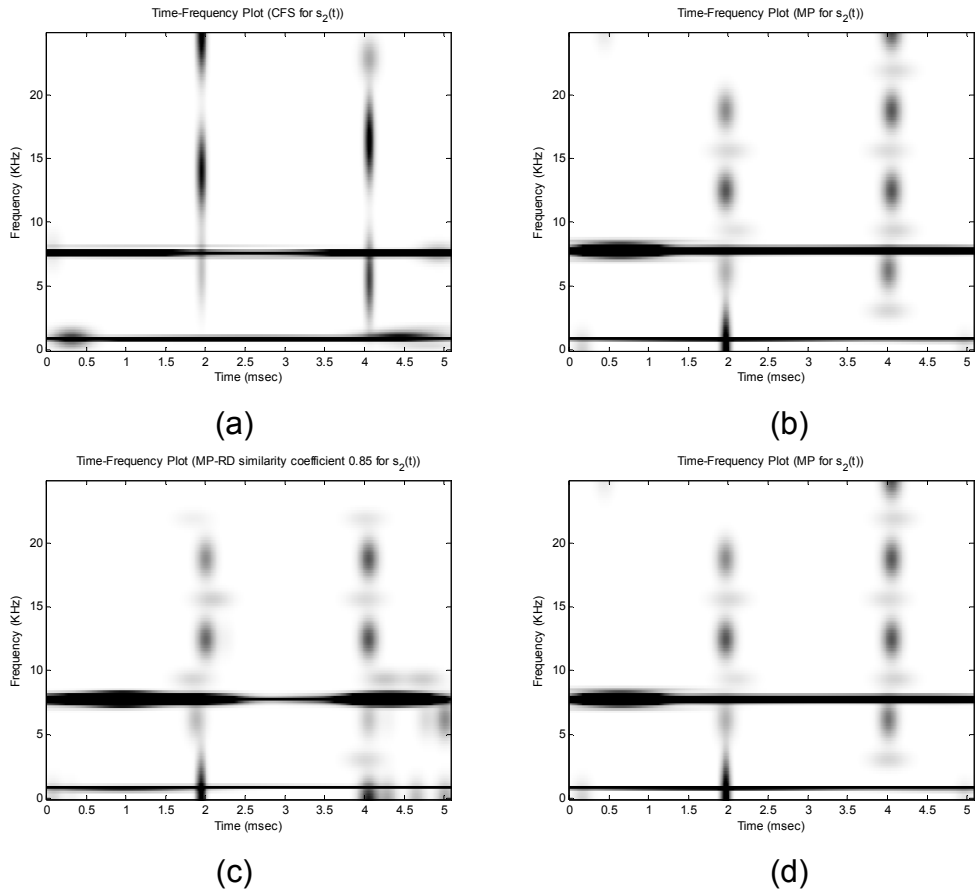

Figure 5.3 : Time-Frequency plots of the sample signal $s_2(t)$.

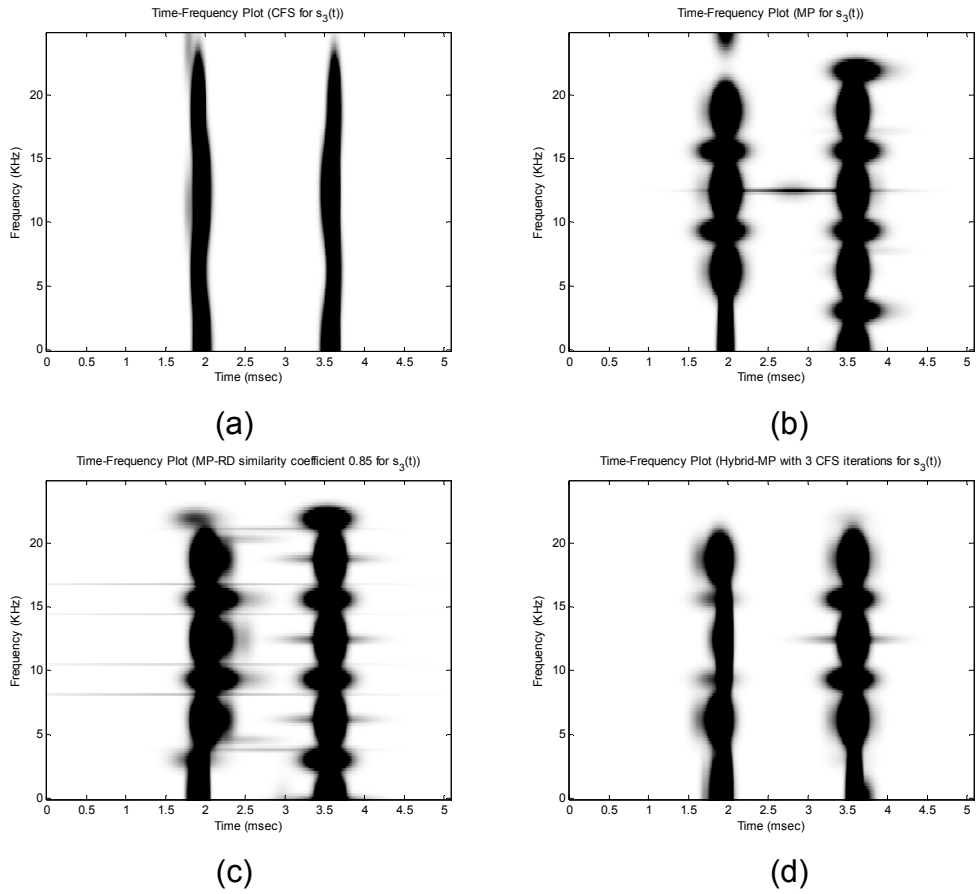

Figure 5.4 : Time-Frequency plots of the sample signal $s_3(t)$.

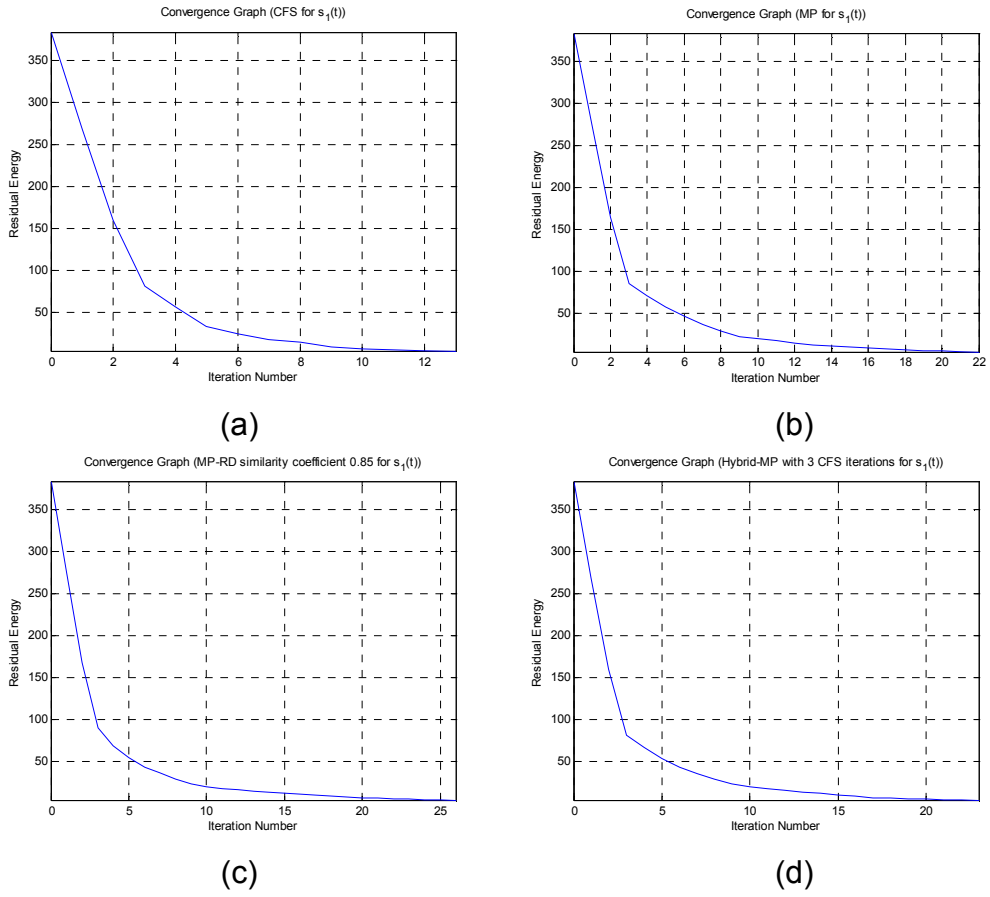

Figure 5.5 : The convergence graphs for the sample signal $s_1(t)$.

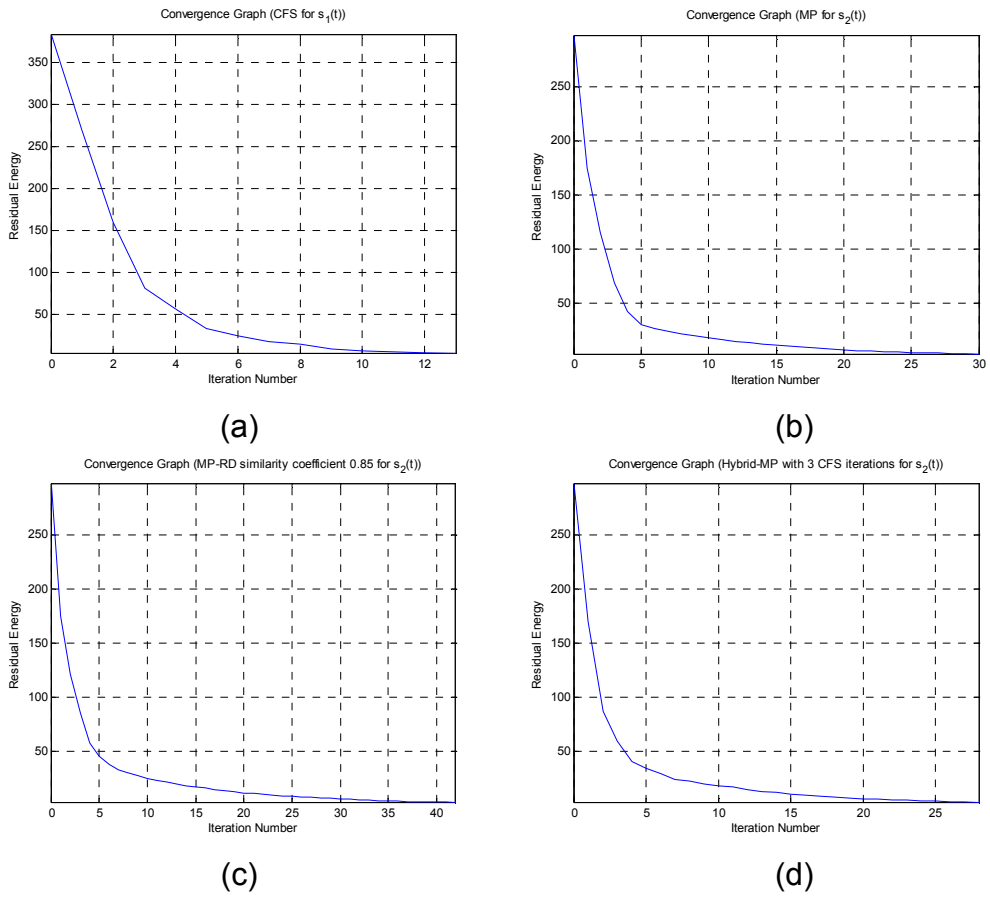

Figure 5.6 : The convergence graphs for the sample signal $s_2(t)$.

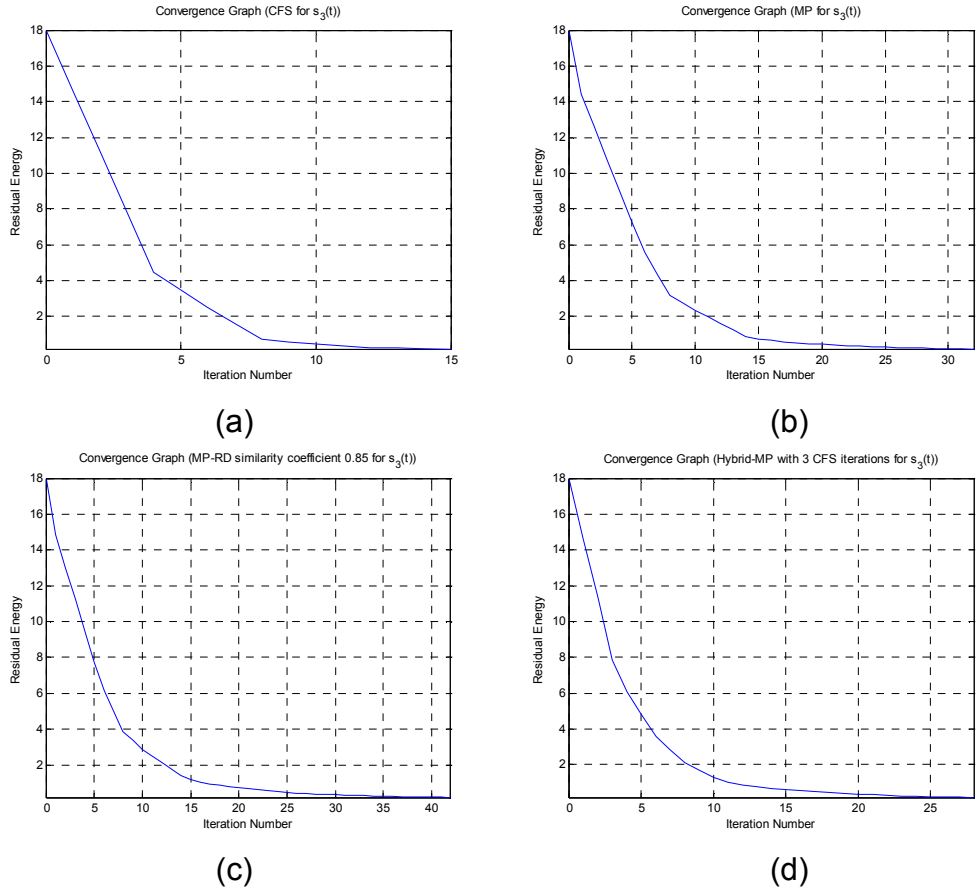

Figure 5.7 : The convergence graphs for the sample signal $s_3(t)$.

5.3 Applications of the AGR on the Target Imaging

The performances of the proposed search algorithms for the AGR are investigated on target imaging system by using the raw data set for the generated aircraft model and MIG-25 frequency signature obtained from the web address; http://airborne.nrl.navy.mil/~vchen/data.

The imaginary aircraft for the simulations is created by the point-scatterer model. The model is generated in 3-D space for better representing the reality. The dimensions of the generated aircraft can be seen in Figure 5.8.

For the simulation, the SF radar is used. The radar pulse is transmitted to the point scatterer model of the aircraft and received back again and the target is moved through a predetermined path. At each pulse, the model of the aircraft is updated according to the path and the received pulses are put into a form for processing in the target imaging system. (See Figure 5.9.) The motion of the model is not restricted by the path but also some rotation effects around the center of the model are applied.

By using two different paths, the model is simulated and two raw data sets, raw data 1 and raw data 2, are generated. Raw data 1 is obtained by using the path given in Figure 5.10. The target is assumed to be moving through a linear path. The center of the target is assumed to be 20,000 meters away from the radar and the altitude of the target is taken as 7,000 meters. A sinusoidal disturbance $w_{yaw_1}(t)$ is created by giving a rotation rate, in degrees per second, around the internal z-axis of the target model,

$$w_{yaw_1}(t) = 7\sin\left(2\pi\frac{1}{10}t\right)$$

The radar is operated with 9 GHz center frequency and 256 MHz bandwidth during the simulation. The number of bursts transmitted is taken as 512; each burst contains 128 pulses with 40 KHz pulse repetition frequency. Therefore, the target is illuminated around 1.64 seconds and 0.56 meters range resolution is obtained.

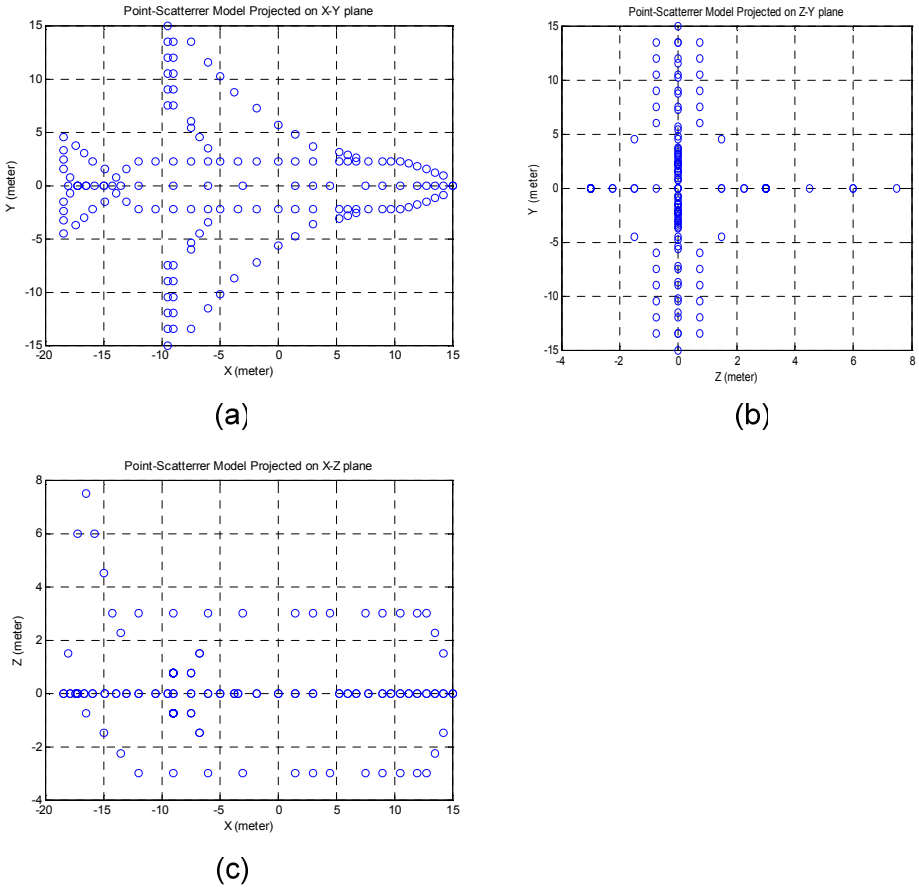

Figure 5.8 : The dimensions of the imaginary aircraft model.

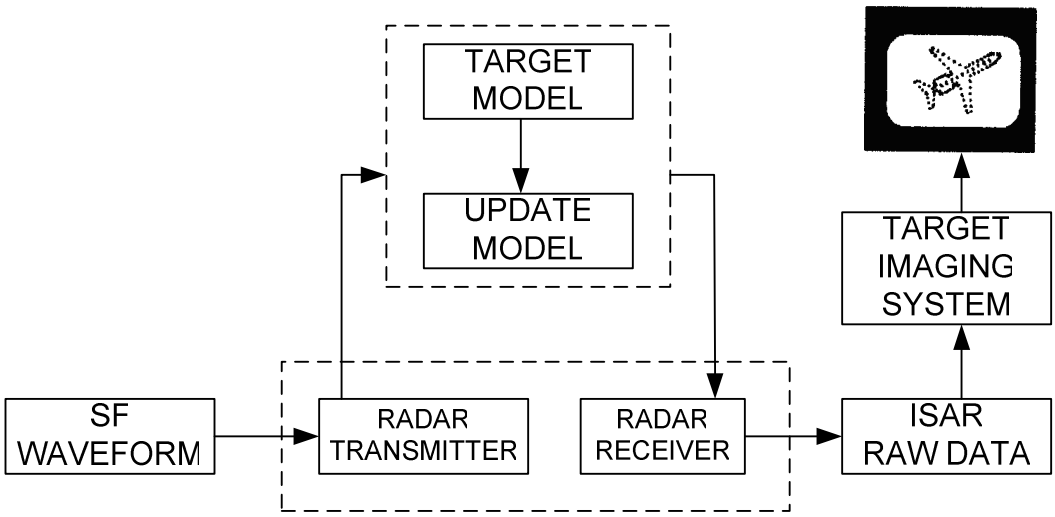

Figure 5.9 : The simulation system of the target model.

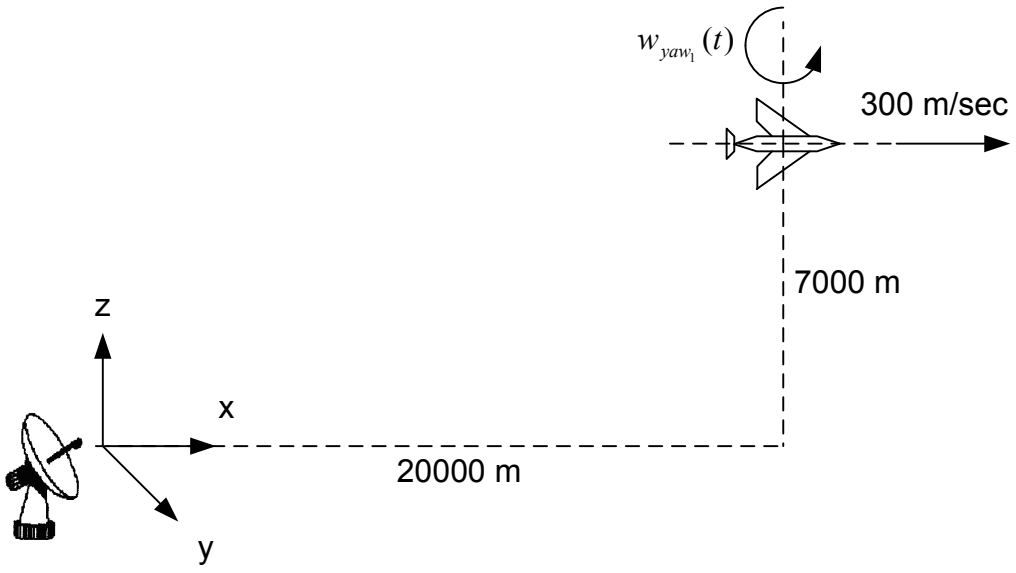

Figure 5.10 : The simulation path 1.

Raw data 2 is created by using the maneuvering path given in Figure 5.11. the target is rotated around a circular path whose center is 40,000 meters away from the radar. The rotation rate of the target through the path is taken as 1 deg/second. The altitude of the target is taken as 7,000 meters. For increasing the complexity of the motion, the yaw rotation rate for the target itself is also taken into account. The given yaw rotation rate in deg/second to the target is,

$$w_{yaw_2}(t) = 10\sin\left(2\pi\frac{1}{15}t\right)$$

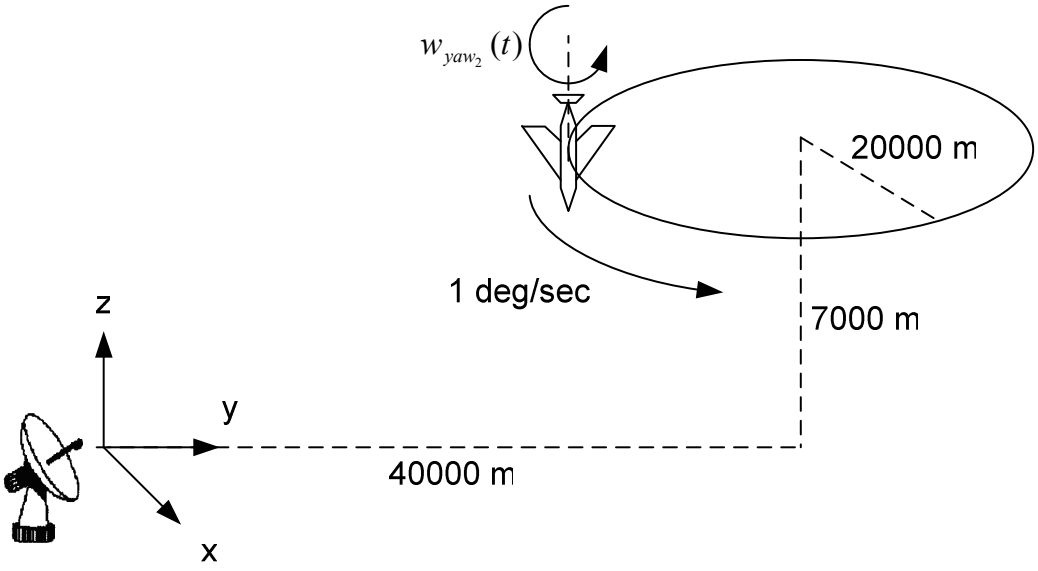

Figure 5.11 : The simulation path 2.

The center frequency for the radar is again taken as 9 GHz, but its bandwidth is increased to 512 MHz. For observing the target, 512 bursts of 128 pulses are transmitted through the target and raw data 2 is obtained. The pulse repetition frequency of the radar is taken as 40 KHz. The total observation time for the

target is 1.64 seconds and the range resolution of the radar is approximately 0.29 meters.

As a third raw data set, raw data 3, the frequency signature of the MIG-25 aircraft is used. Like raw data 1 and raw data 2, raw data 3 is obtained by simulation. The center frequency of the radar is taken as 9 GHz and the bandwidth of the radar as 512 MHz. The pulse repetition frequency is given as 15 KHz with 512 successive pulses contained in 64 bursts.

5.4 Target Imaging by 2-D Fourier Transform

Firstly, the obtained raw data sets are used in conventional target imaging system which uses the 2-D Fourier transform for differentiating the Doppler information in the data set. Since the Doppler information of the data sets is time-varying, the obtained images are degraded by smearing and blurring effects [14][20]. Therefore, the details of the images are suppressed by the insufficiency of the conventional target imaging method for representing the Doppler shift. The time-invariant Doppler shift is not possible even for targets with constant rotation rates for row, pitch or yaw rotations. The images of the maneuvering target will almost be degraded by time-varying Doppler shift if obtained by 2-D Fourier transform without any sophisticated range and Doppler tracking algorithms [20]. Although the signal processing time for the conventional method is very short, the obtained results may not be acceptable. (See Figure 5.12.)

Table 5.2 : Target Imaging times for 2-D FFT in seconds.

IMAGING METHOD	RAW DATA 1	RAW DATA 2	RAW DATA 3
2-D FFT	0.033	0.031	0.032

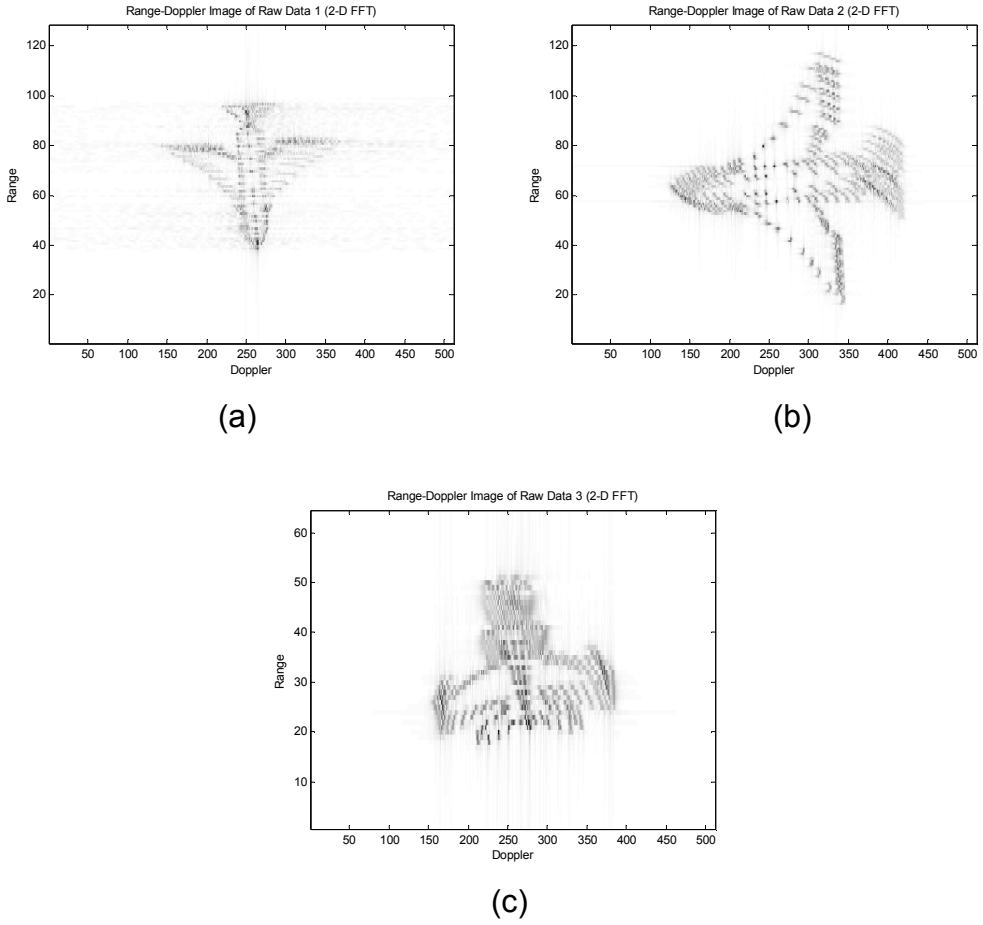

Figure 5.12 : The Range-Doppler Images of data sets by 2-D FFT.

5.5 Target Imaging by Adaptive Gabor Representation with Coarse-to-Fine Search

The produced data sets are used in target imaging method utilizes the AGR with the CFS Algorithm. (See Figure 5.13.) The signals in the data sets are decomposed until the energy of the remainder signals is less than or equal to 1/10 of the original signals. Figure 5.14 - Figure 5.16 show the target images for raw data 1, raw data 2 and raw data 3 obtained by the AGR with the CFS Algorithm.

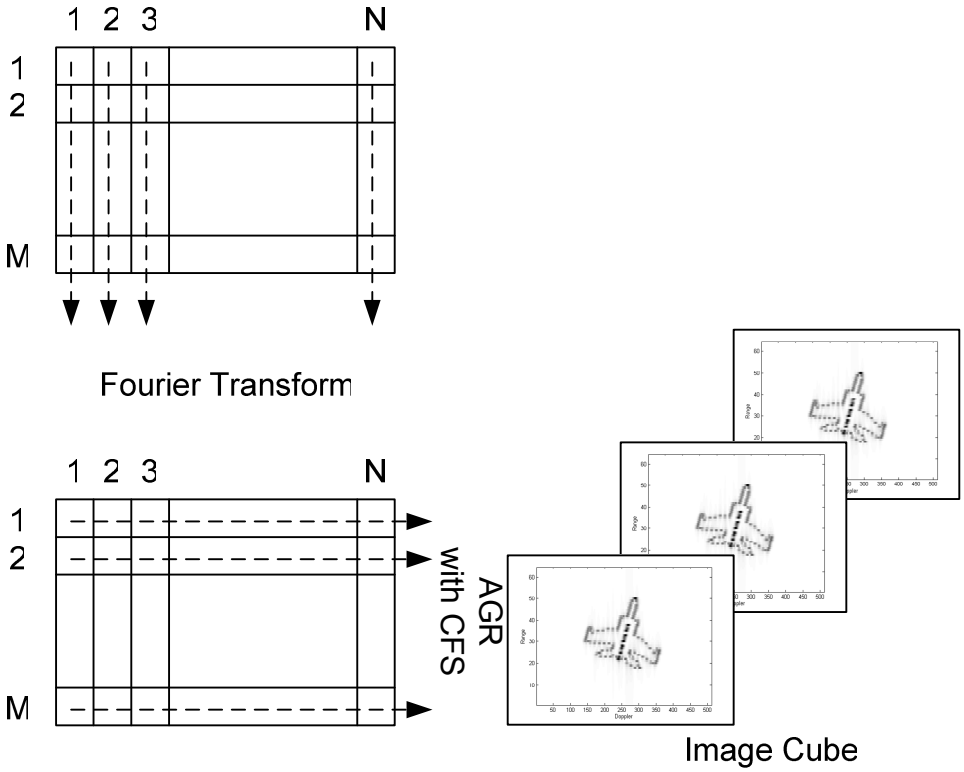

Figure 5.13 : Application of the AGR with CFS for target imaging.

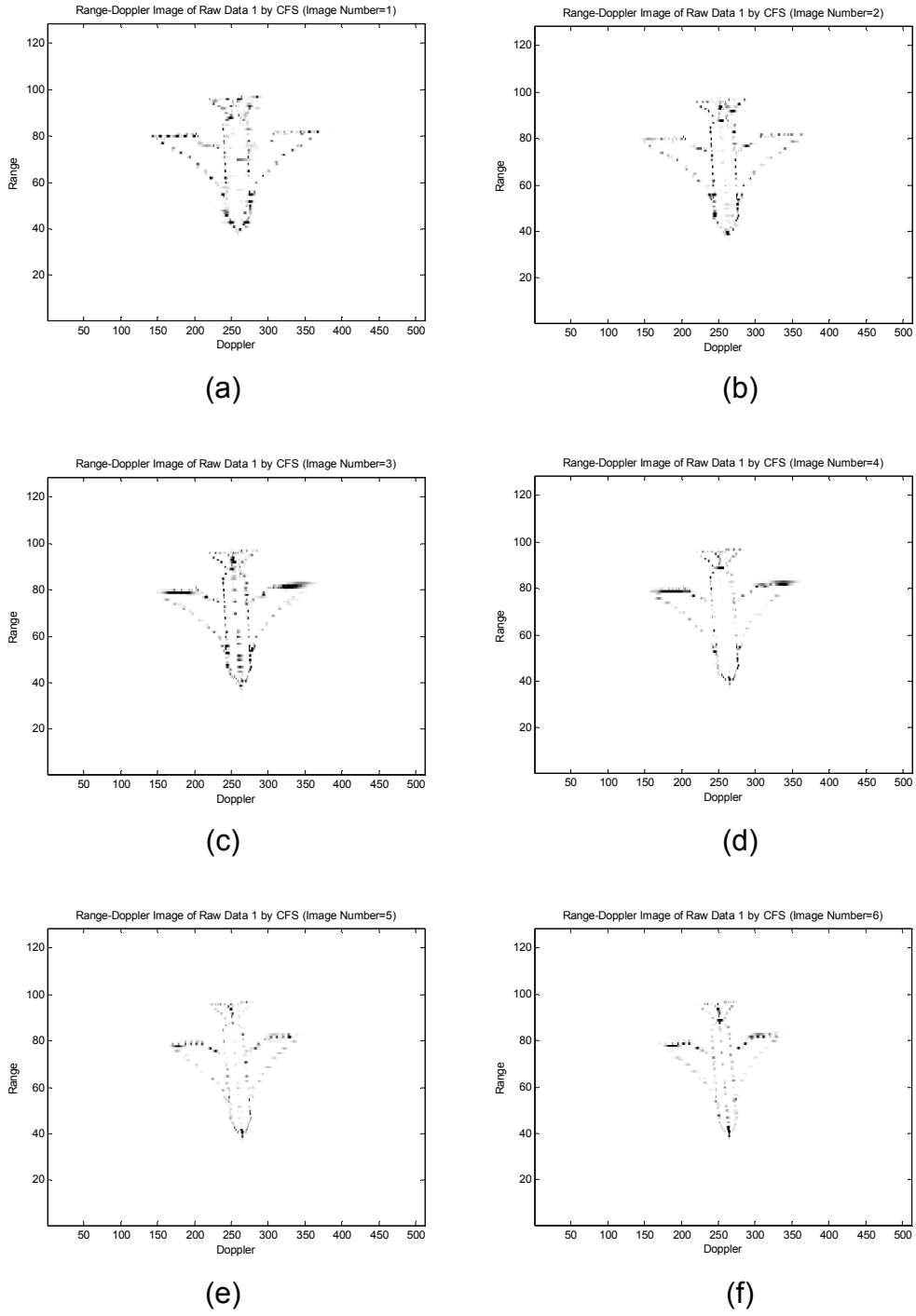

Figure 5.14 : The Range-Doppler images of raw data 1 by AGR CFS.

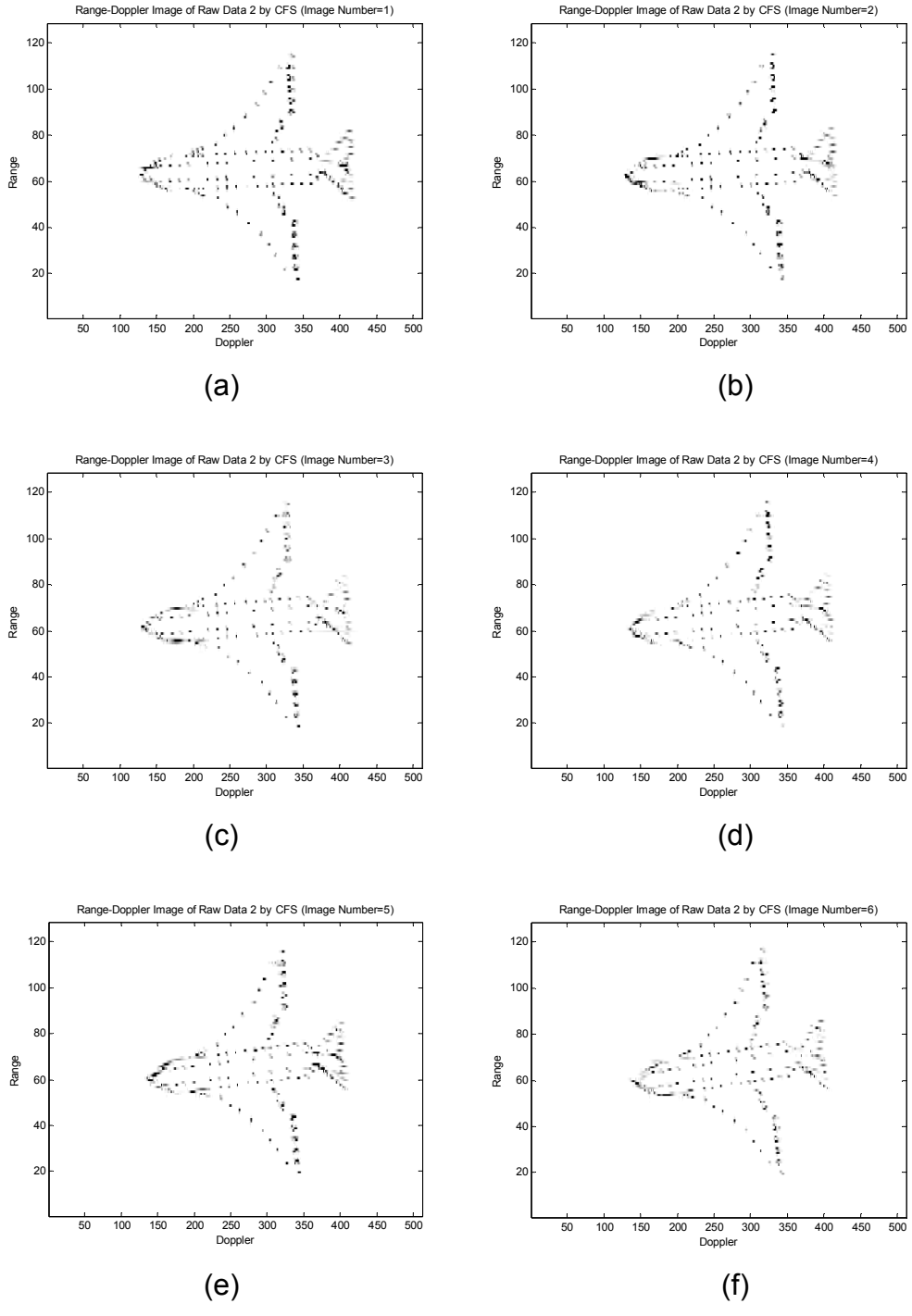

Figure 5.15 : The Range-Doppler images of raw data 2 by AGR CFS.

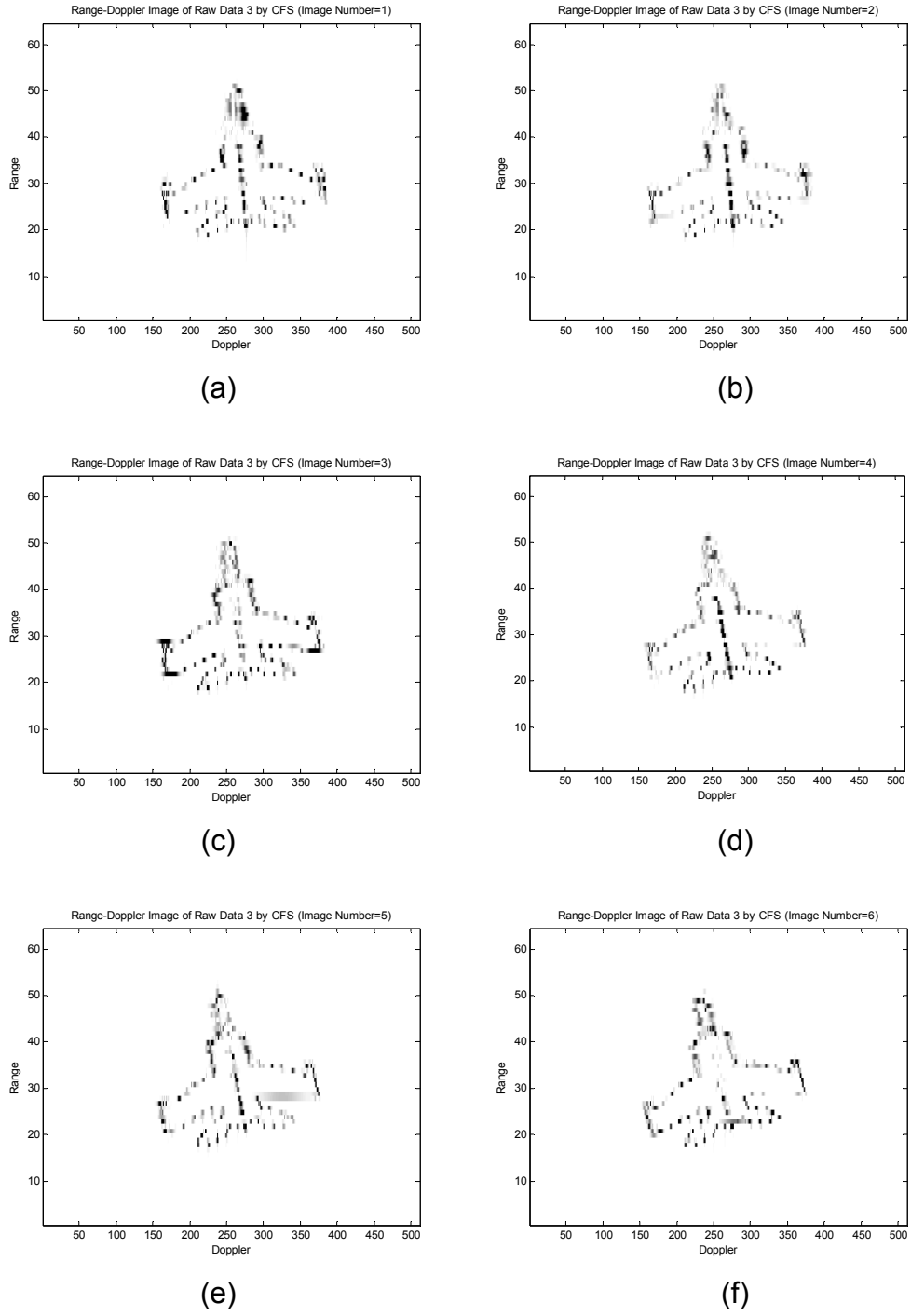

Figure 5.16 : The Range-Doppler images of raw data 3 by AGR CFS.

5.6 Target Imaging by Adaptive Gabor Representation with Matching Pursuit with Reduced Dictionary Search

The produced data sets are used in target imaging method utilizes the AGR with the MP-RD Search Algorithm. (See Figure 5.17.) The signals in the data sets are decomposed until the energy of the remainder signals is less than or equal to 1/10 of the original signals. The function dictionary is composed by taking the similarity coefficient as 0.75. Figure 5.18 - Figure 5.20 show the target images for raw data 1, raw data 2 and raw data 3 obtained by the AGR with the MP-RD.

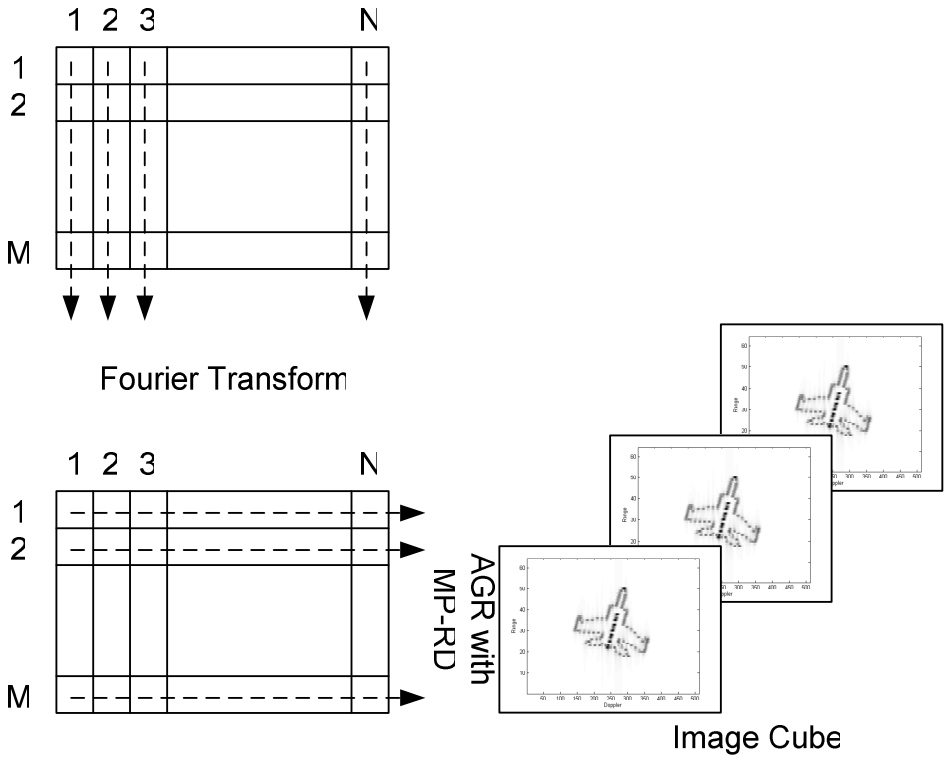

Figure 5.17 : Application of the AGR with MP-RD for target imaging.

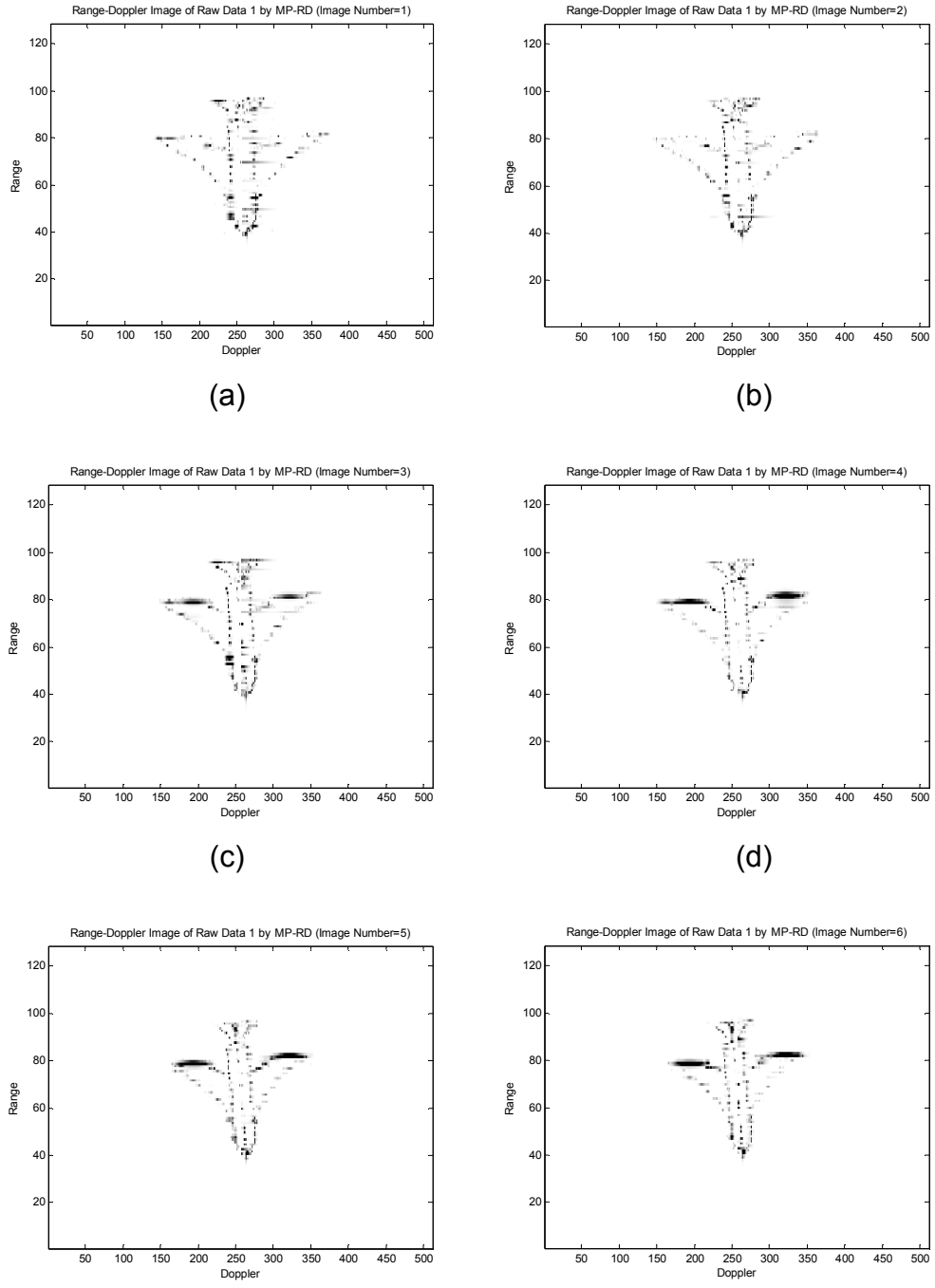

Figure 5.18 : The Range-Doppler images of raw data 1 by AGR MP-RD.

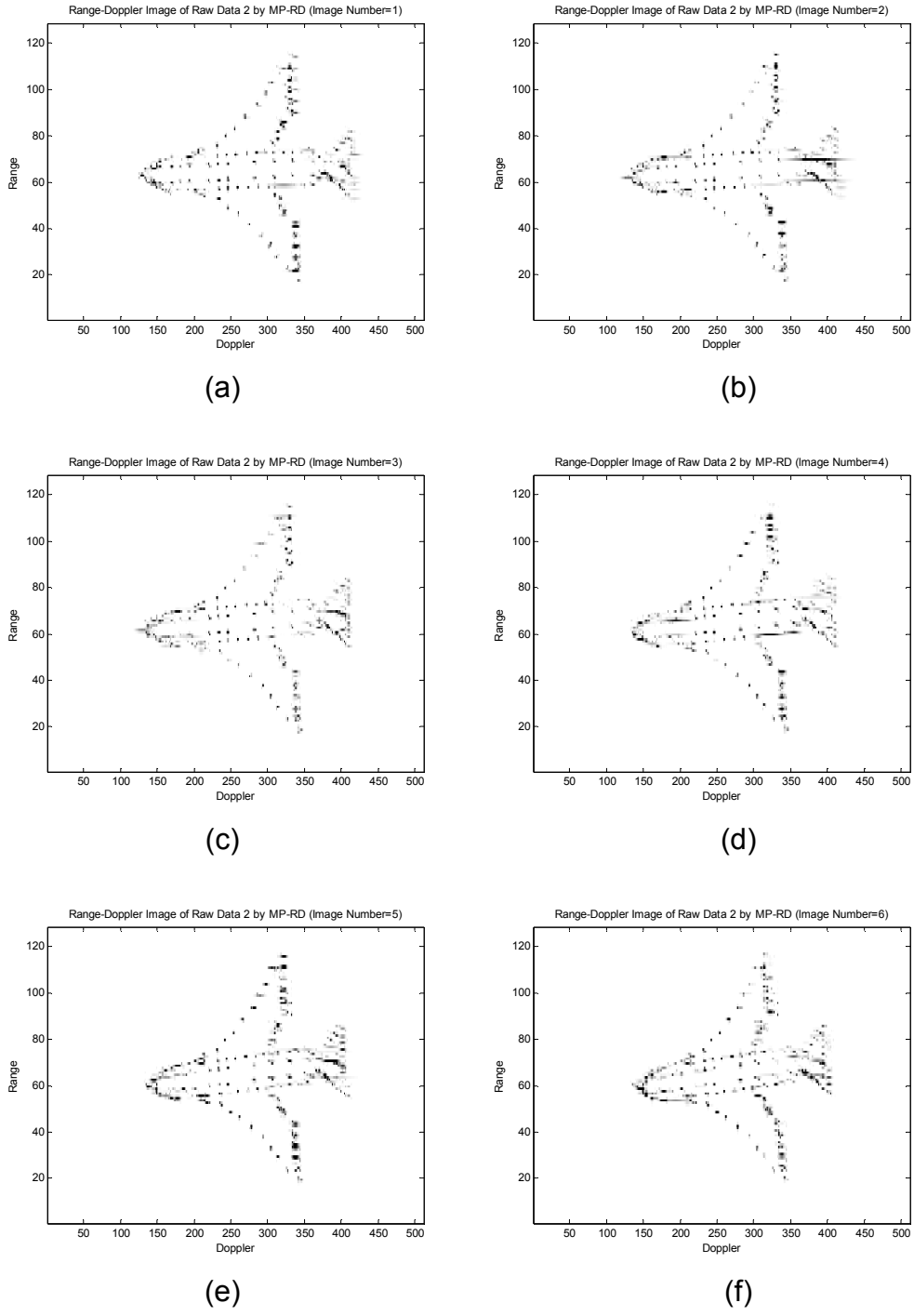

Figure 5.19 : The Range-Doppler images of raw data 2 by AGR MP-RD.

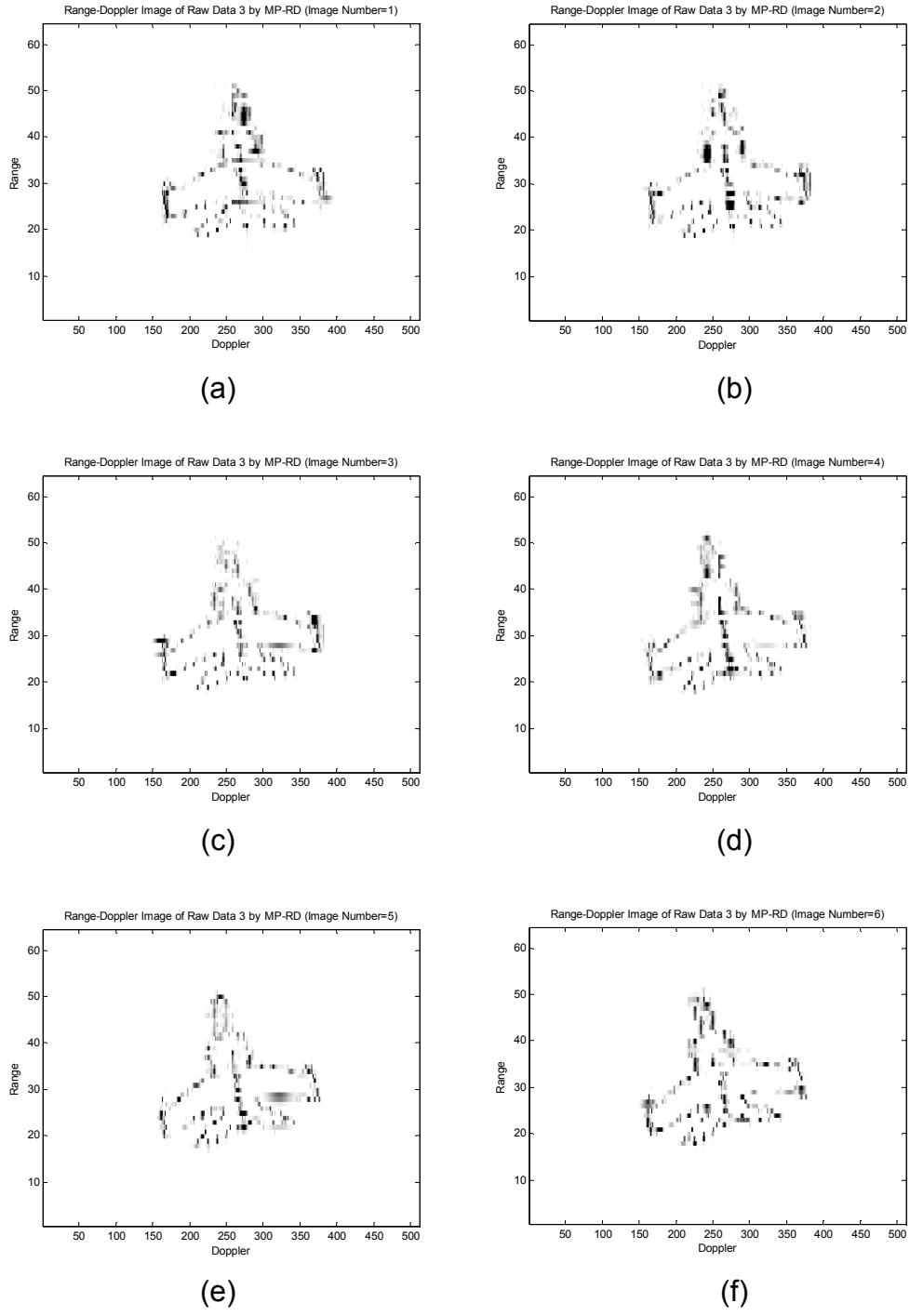

Figure 5.20 : The Range-Doppler images of raw data 3 by AGR MP-RD.

5.7 Target Imaging by Adaptive Gabor Representation with Hybrid Matching Pursuit

The produced data sets are used in target imaging method utilizes the AGR with the Hybrid MP Search Algorithm. (See Figure 5.21.) The signals in the data sets are decomposed until the energy of the remainder signals is less than or equal to 1/10 of the original signals. The function dictionary is composed by taking the similarity coefficient as 0.75. The CFS Algorithm is iterated for 3 times before the MP-RD Algorithm. Figure 5.22 - Figure 5.24 show the target images for raw data 1, raw data 2 and raw data 3 obtained by the AGR with the Hybrid MP.

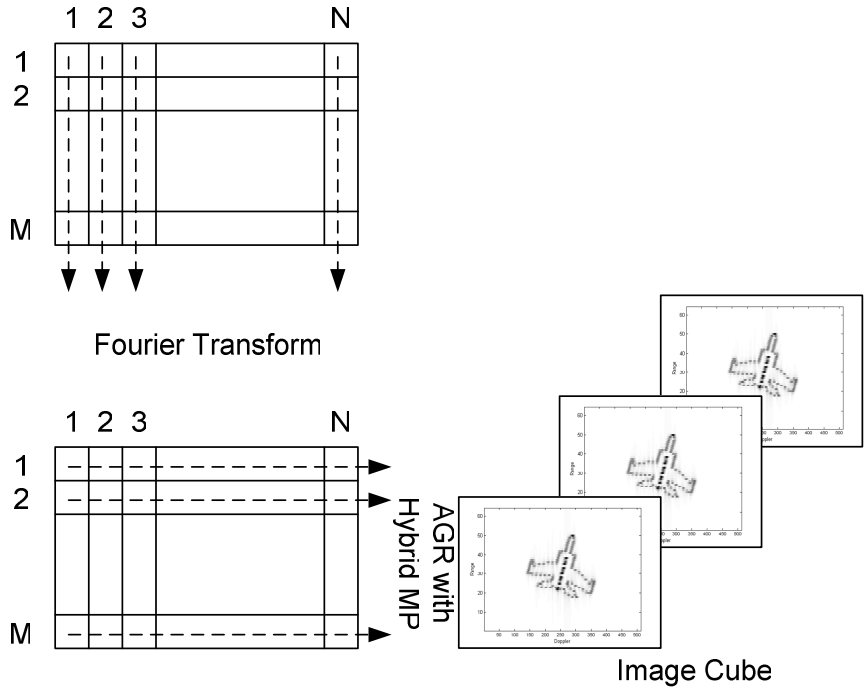

Figure 5.21 : Application of the AGR with the Hybrid MP for target imaging.

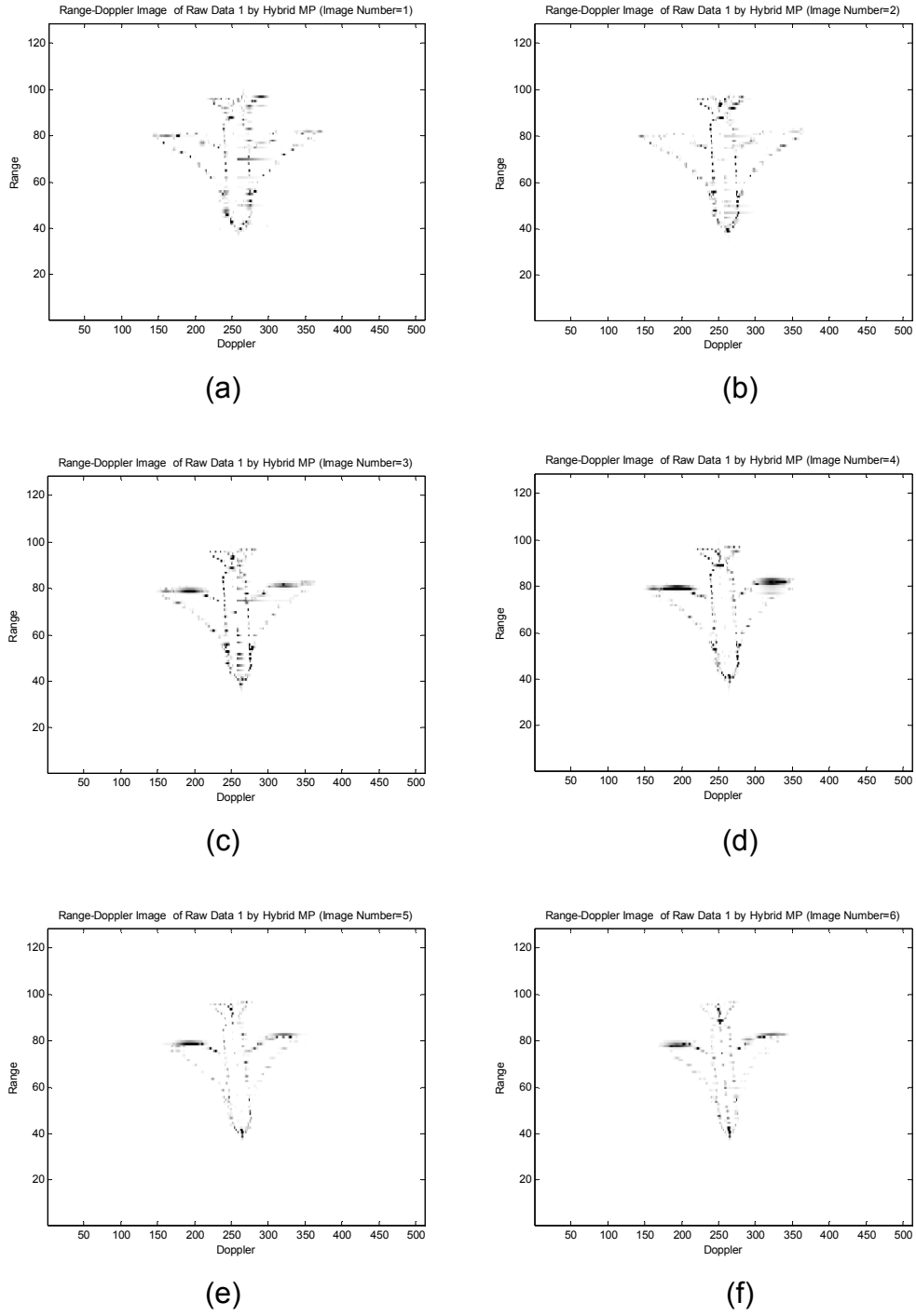

Figure 5.22 : The Range-Doppler images of raw data 1 by AGR Hybrid MP.

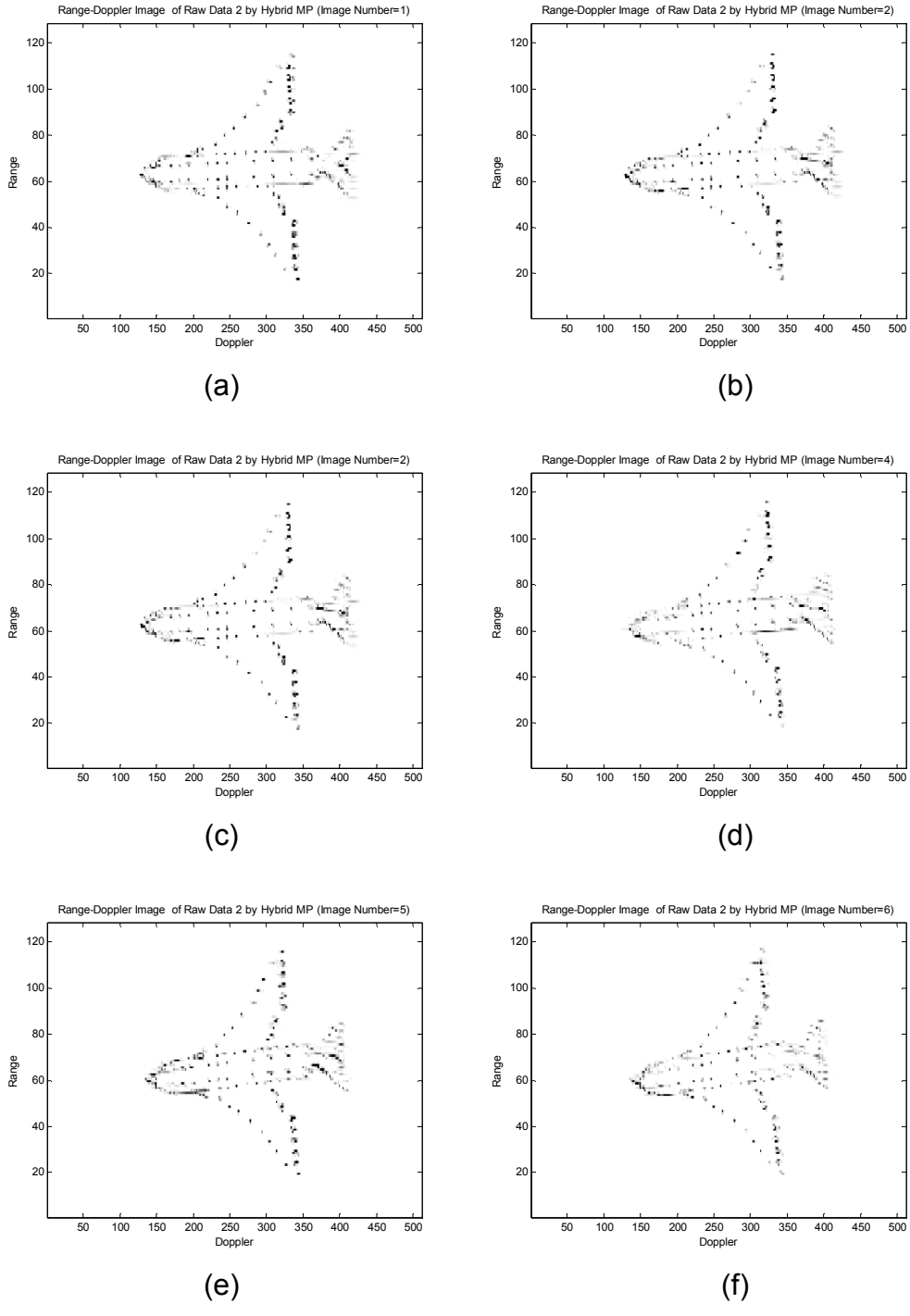

Figure 5.23 : The Range-Doppler images of raw data 2 by AGR Hybrid MP.

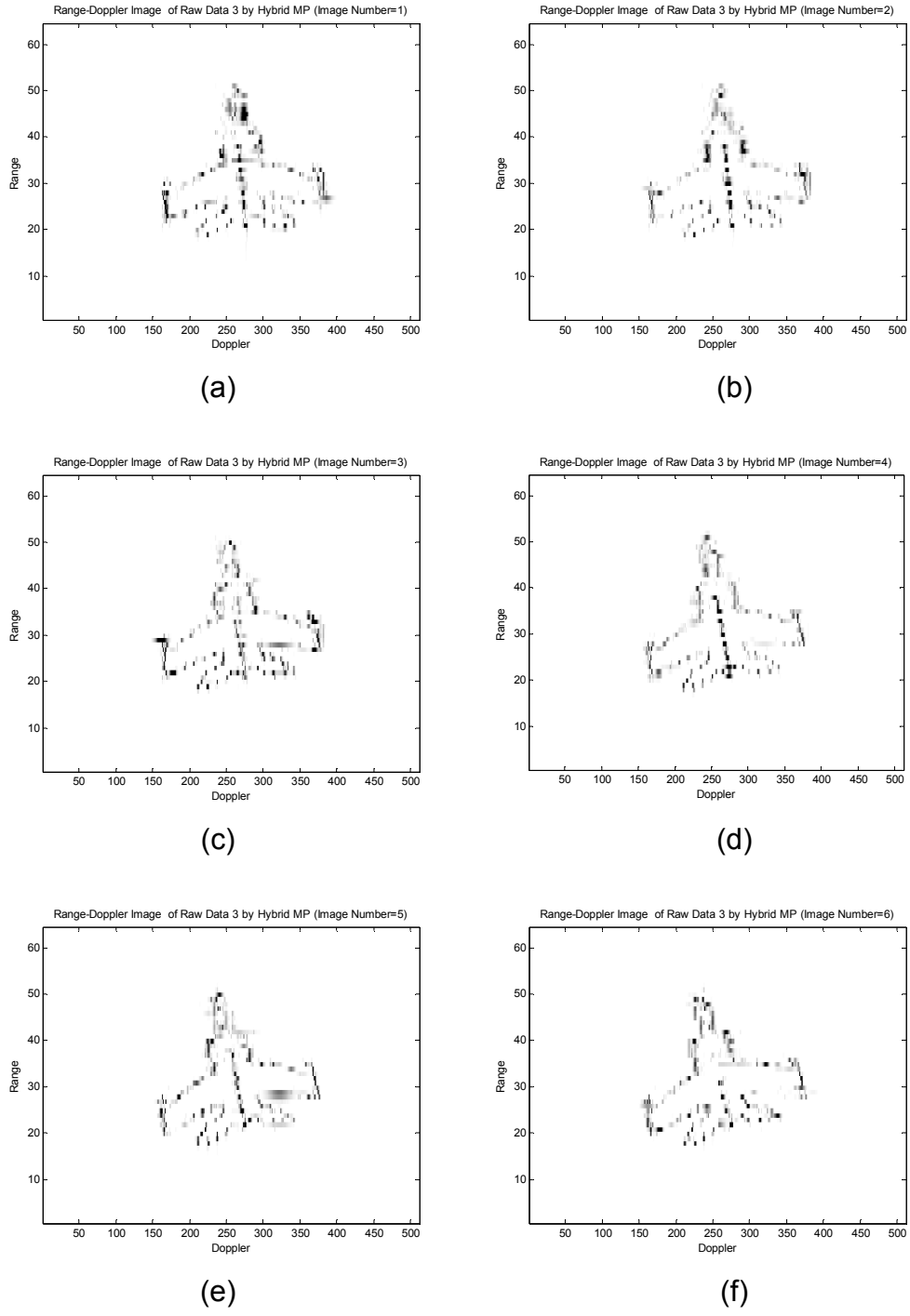

Figure 5.24 : The Range-Doppler images of raw data 3 by AGR Hybrid MP.

5.8 Timing Analysis of the Methods

The quality of the images is very good for the AGR with the CFS. The smearing effect of the time-varying Doppler shift is almost phased out and the blurring is suppressed much [14]. Therefore, the power of the time-frequency transform techniques in the target imaging application is presented. On the other side, the processing time is drastically reached to enormous amount by the CFS Algorithm. The advantages of the AGR loose the meaning with very long signal processing time. (See Table 5.3.)

The MP-RD method creates an opportunity for the usage of the AGR. Although the resolution of the images is worse, the signal processing time is pulled down to feasible value. If the improved resolution is also desired in addition to the speed, the Hybrid MP Algorithm can be used, noting that the processing time difference between the MP-RD and the Hybrid MP methods is tolerable.

Table 5.3 : Target imaging times in seconds for the AGR.

IMAGING METHOD	RAW DATA 1	RAW DATA 2	RAW DATA 3
AGR CFS	88.609	55.016	40.234
AGR MP-RD	30.437	23.735	13.093
AGR Hybrid MP	31.500	24.753	15.453

CHAPTER 6

CONCLUSIONS

The radar can be used for not only detection of the target but also imaging it. ISAR technique makes the target imaging possible. If the target is taken as composed of point scatterers, the target imaging system tries to locate the scatterers onto the Range-Doppler plane. As a result, a scaled version of the shape of the target can be constructed on the Range-Doppler plane.

The main concern in target imaging is extracting the Doppler information from the received radar waveform. The range resolution of the radar determines the locations of the point scatterers along the LOS. The locations of the scatterers along the cross-range direction are determined by the Doppler shift of the scatterers. In this work, the conventional target imaging method and an advanced imaging method which uses the time-frequency transform techniques are investigated.

Firstly, the conventional target imaging method is examined. The simplest and the fastest method uses the Fourier transform for extracting the Doppler shift information form the received radar pulses. Although the method is very efficient and simple under certain circumstances, the efficiency of the method depends on the motion of the target. If target exhibits a complex motion, like maneuvering, the Doppler spectra of the scatterers will be time-varying and a point scatterer may move through more than one resolution cell during the target observation time. Hence the Range-Doppler image obtained by the Fourier transform will be

degraded. The smearing and blurring effects on the image destroy the details of the image for identification. Therefore, a sophisticated range tracking algorithm should be applied for yielding reasonable results by the conventional target imaging method.

Obtaining clear images is made possible by using a proper time-frequency transform without using range tracking algorithm other than global motion compensation. One of the best candidates for the time-frequency transform techniques is the Wigner-Ville Distribution. The WVD is a high resolution time-frequency technique which can show the frequency content of the signal with high accuracy. Although the WVD has many useful properties, directly applying the WVD is not possible, in most cases, because of the cross-term interference.

By adaptive representation, the WVD can be used in spectral analysis of the signals. After the signal is re-produced in terms of the elementary functions, the WVD can be used without suffering from the cross-term interference. As a second target imaging technique, the range profiles of the target are decomposed by adaptive representation with the Gabor elementary functions, AGR, and the WVD is used. Then the obtained spectrogram, AS, is used in the image construction and the obtained images were good enough for showing the merit of the time-frequency transform in the target imaging application.

On the contrary, the main concern in the AS is finding the best elementary functions for representation. Three different searching algorithms are used and compared. The first one is the CFS Algorithm. The algorithm starts with a Gabor function of large variance and tries to find the best match by reducing the variance at each step. Although the obtained images have almost the best image quality and the time-frequency resolution, the main drawback of the algorithm is the signal processing time.

For reducing the processing time, the MP can be an alternative searching method. In the MP, the elementary function search is limited by a pre-selected function dictionary. Since the time consuming inner product operations are for once, the speed in the processing time can be achieved by the MP. On the other side, the constructed function dictionary needs much memory and requires the management of a huge data for the image construction. Hence, by reducing the number of elements in the function dictionary, the MP-RD method is developed. As a second search method, the MP-RD is applied on the AGR, and it is indicated that the MP-RD is almost three times much faster search algorithm than the CFS.

On the other hand, the target images obtained by the AGR with the MP-RD suffer from smearing effect a little. Although the obtained results by the MP-RD are still pretty good for target identification, the method is supported by the CFS and the Hybrid MP Algorithm is developed by combining the merit sides of the two different methods, the CFS and the MP-RD. The remainder signal of the CFS Algorithm is used again in the MP-RD Algorithm. Hence the time-frequency resolution of the CFS Algorithm and the speed of the MP-RD Algorithm are projected on to the obtained target images. The signal processing times of the Hybrid MP Algorithm do not drift out from those of the MP-RD Algorithm, and the image quality of the MP-RD Algorithm is enhanced through the image quality of the CFS Algorithm.

In the future, the performance of an alternative search method, the Basis Pursuit, can be tested for the target imaging systems. Since the used function dictionary contains independent elements, the redundancy of the dictionary is phased out. Therefore, it can be expected that the signal processing time will decrease with the resolution on the target image. Beside a new search technique, the advantages of the time-frequency transform can be tried to be used in the range tracking algorithm for the conventional target imaging. Since the Fourier transform

constructs the target image in a much shorter time from any time-frequency transform technique, enhancements in the range tracking may bring advantages to the conventional target imaging system.

REFERENCES

[1] D.A.Ausherman, A.Kozman, J.L.Walker, H.M.Jones, E.C.Poggio, "Developments in Radar Imaging", IEEE Transactions on Aerospace and Electronic Systems, AES-20, No.4, July 1984.

[2] H.Choi, A.W.Krone, D.C.Munson, "ISAR Imaging of Approaching Targets", IEEE ICASSP, San Fransisco, CA, March 23-26 1992.

[3] D.C.Munson, J.D.O'Brien, W.K.Jenkins, "A Tomographic Formulation of Spotlight-Mode Synthetic Aperture Radar", Proceedings of the IEEE, Vol.71, No.8, August 1983.

[4] L.Cohen, "Time-Frequency Analysis", Prentice Hall, 1995.

[5] D.R.Wehner, "High-Resolution Radar", 2nd ed., Artech House, 1995.

[6] J.L.Walker, "Range-Doppler Imaging of Rotating Objects", IEEE Transactions on Aerospace and Electronic Systems, AES-16, No.1, January 1980.

[7] J.C.Goswami, A.K.Chan, "Fundamentals of Wavelets", John Wiley & Sons Ltd., 1999.

[8] V.C.Chen, S.Qian, "Joint Time-Frequency Transform for Radar Range-Doppler Imaging", IEEE Transactions on Aerospace and Electronic Systems, Vol.34, No.2, April 1998.

[9] S.Qian, D.Chen, "Joint Time-Frequency Analysis - Methods and Application", Prentice Hall, 1996.

[10] S.Qian, D.Chen, "Signal Representation Using Adaptive Normalized Gaussian Function", Signal Processing, 36(1), pp1-11, 1994.

[11] V.C.Chen, "Adaptive Time-Frequency ISAR Processing", SPIE, Vol.2845/133.

[12] M.W.Van Zyl, M.R.Inggs, "Inverse Synthetic Aperture Radar Images of Moving Targets", IEEE, 1991.

[13] F.Berizzi, M.Diani, "ISAR Imaging of Rolling, Pitching and Yawing Targets", IEEE, 1996.

[14] Y.Ding, N.Xue, D.C.Munson, "An Analysis of Time-Frequency Methods in ISAR Imaging of Moving Targets", IEEE, 2000.

[15] F.Berizzi, M.Diani, "Target Angular Motion Effects on ISAR Imaging", IEEE Proc. Radar, Sonar Navig., Vol.144, No.2, April 1997.

[16] S.Qian, D.Chen, "Decomposition of Wigner-Ville Distribution and Time-Frequency Distribution Series", IEEE, 1994.

[17] S.Mallat, Z.Zhang, "Matching Pursuit with Time-Frequency Dictionaries", IEEE Transactions in Signal Processing, December 1993.

[18] V.C.Chen, H.Ling, "Time-Frequency Transform for Radar Imaging and Signal Analysis", Artech House, 2002.

[19] H.Choi, "Signal Processing Issues in Synthetic Aperture Radar and Computer Tomography", Ph.D. Thesis, 1998.

[20] A.Jain, "SAR/ISAR Imaging of a Nonuniformly Rotating Target", IEEE Transactions on Aerospace and Electronic Systems, Vol.28, No.1, January 1992.